Direct vibrational energy transfer in zeolites

Brugmans, M.J.P.; Bonn, M.; Bakker, H.J.; Lagendijk, A.

DOI
10.1063/1.470876
Publication date
1996

Published in
Journal of Chemical Physics

Direct vibrational energy transfer in zeolites

Marco J. P. Brugmans, Huib J. Bakker, and Ad Lagendijk
FOM-Institute for Atomic and Molecular Physics, Kruislaan 407, 1098 SJ Amsterdam, The Netherlands

(Received 14 June 1995; accepted 29 September 1995)

With two-color picosecond infrared laser spectroscopy the dynamics of O–H and O–D stretch vibrations in zeolites are investigated. Zeolites appear to be good model systems to study transfer of vibrational energy in a solid. For the O–D vibrations, transient spectral holes are burnt in the inhomogeneously broadened absorption bands by saturating the absorption with a strong pump pulse. From the spectral hole widths the homogeneous absorption linewidths are obtained. The excited population lifetimes are determined using a time-resolved pump–probe technique, and in combination with the homogeneous linewidth the pure dephasing time is revealed as well. For high concentrations of O–H oscillators the vibrational stretch excitations are found to diffuse spectrally through the inhomogeneous absorption band. This spectral diffusion process is explained by direct site-to-site transfer of the excitations due to dipole–dipole coupling (Förster transfer). The dependences of the transient spectral signals on oscillator concentration and the results of one-color polarization resolved experiments confirm this explanation. The spectral transients are satisfactorily described by simulations in which the site-to-site transfer by dipole–dipole coupling is taken into account. © *1996 American Institute of Physics.* [S0021-9606(96)03701-3]

I. INTRODUCTION

With the advent of intense picosecond mid-infrared laser pulses, it has become possible to study the population dynamics of molecular vibrations in the condensed phase in a time-resolved way, directly revealing excited-state lifetimes and energy pathways of vibrational energy (see Ref. 1 for an early review). This information cannot be obtained in the frequency domain, because inhomogeneous broadening and (at room temperature) pure dephasing mechanisms are usually the main contributions to the absorption lines. Hence, ultrafast infrared spectroscopy is essential to achieve a fundamental understanding of vibrational dynamics in the condensed phase.

The vibrational dynamics of small molecules in solution have extensively been studied with ultrafast infrared spectroscopy (see Refs. 2–14 for some examples). These experiments have provided insight into intramolecular and intermolecular energy transfer processes in the liquid phase[2–5,8–13] as well as in the dissociation dynamics of hydrogen bonds.[6,7,14] To investigate the vibrational coupling between adsorbates and surfaces, the same time-resolved techniques have been applied to adsorbates.[15–27] The population dynamics of molecular vibrations in solid matrices containing some disorder[28–33] have received less attention so far. It is interesting to study these dynamics from a fundamental point of view, because the collective effects and vibrational couplings can be expected to be important in these systems. The different environments of the vibrational oscillators in these solids lead to inhomogeneous broadening of the absorption bands so that a straightforward interpretation of the results in single-molecule properties is difficult. As a consequence, interesting phenomena like spectral diffusion might occur in these systems.

Another challenge is to apply the time-resolved spectroscopic techniques to chemically active systems to learn more about the chemical dynamics and reactions (see, e.g., Ref. 34 and references therein). In this context the population dynamics of hydroxyl vibrations in zeolites have been studied in the last few years.[35–43] Acid zeolites are industrially important materials because they are widely exploited as catalysts.[44] Catalytically active sites in the porous zeolite framework are the hydroxyl groups, which are found near aluminum atoms in the crystalline alumino-silicate structure. The time-resolved infrared saturation experiments provided new information on the different hydroxyl groups and hydrogen bonding to the lattice,[37,38] on the deexcitation mechanism,[42] and on interactions with adsorbates.[43] Besides contributing to the insight in the molecular structure, these studies are the very first step in revealing the reaction dynamics on a molecular scale, since the coordinate of the hydroxyl stretch vibration is parallel with the reaction coordinate for the catalytic proton donation.[45]

The main objective of the present study is to gain insight into population dynamics of molecular vibrations embedded in a crystalline host, for which the zeolites have proven to be good model systems. We investigate the vibrational dynamics of hydroxyl groups in zeolites in detail with double resonance picosecond spectroscopy.[2,5] This two-color infrared technique permits us to directly follow energy pathways and couplings between different vibrational modes.

With infrared transient hole-burning techniques (see also Refs. 9, 31, and 32) we have burnt spectral holes in the hydroxyl absorption bands in the zeolites, revealing the inhomogeneity of the hydroxyl sites. From the spectral holes the homogeneous linewidths are determined. With a time-dependent pump–probe technique the rate of population decay is measured. Hence all temporal and spectral information about the vibrations is obtained. We find that at high concentrations of O–H oscillators the vibrational stretch excitations migrate through the inhomogeneously broadened absorption bands on a picosecond time scale. This migration is due to

 0021-9606/96/104(1)/64/21/$6.00

nonradiative dipole–dipole coupling and has extensively been studied for *electronic* excitations.[46–48] For instance, in photosynthetic systems the excitations are transferred by this mechanism.[49,50] For vibrations, this direct excitation transfer was recently found to occur among adsorbates on a surface.[24–26] The notion that at high oscillator concentrations the vibrational excitations in a zeolite hop between different sites is confirmed by experiments in which the oscillator density is varied and by polarization resolved experiments. The transient signals are modeled with simulations in which the direct transfer of the excitations due to dipole–dipole coupling of the oscillators is accounted for.

II. EXPERIMENT

A. Time-resolved two-color infrared saturation spectroscopy

The high-intensity picosecond infrared pulses used for the time-resolved saturation experiments are generated by means of parametric generation and parametric amplification in $LiNbO_3$ crystals.[51,52] To obtain pump and probe pulses which are independently tunable in wavelength,[5] the setup as described in Ref. 10 is extended with another infrared generating branch. An actively and passively mode-locked Nd:YAG laser which delivers 35 ps pulses at 1064 nm with pulse energies up to 60 mJ at a repetition rate of 10 Hz, is used to pump two identical mid-infrared generating laser branches. The YAG pulses are split using HEL (high energy laser) beamsplitters. The pump pulses at frequency ω_3 are downconverted into two other infrared pulses at smaller frequencies ω_1 and ω_2 ($\omega_3=\omega_1+\omega_2$). By angle tuning of the $LiNbO_3$ crystals, frequencies in the range of 2200–7200 cm^{-1} can be generated with this setup. By convention, the wave at the largest frequency ω_1 is called the signal and ω_2 is called the idler. The idler is used for the time-resolved experiments.

Each of the two parametric generation and amplification laser branches, denoted with "1" and "2" in Fig. 1, consists of three (5- or 3-cm-long) $LiNbO_3$ crystals, with the optical axes cut at 47.1°. In each branch, the first crystal is pumped with about 10 mJ of the Nd:YAG pulse energy. The signal and idler waves generated in the first crystal are amplified further in the second crystal using the remaining part of the pump pulses. Behind the second crystal the pump pulse is reflected out of the beam and the idler wave is blocked using a high-pass filter.[10] In the third crystal the signal pulse has temporal overlap with a fresh Nd:YAG pump pulse of about 8 mJ pulse energy and is amplified further. In the same process, a high-intensity idler pulse is generated. The parametric amplification process in the third crystal is in saturation, which reduces the amplitude noise of the generated infrared pulses. Behind the third crystal the remaining pump pulse is reflected out of the beam. The signal pulses are reflected from the beam with dichroic mirrors and are used for diagnostics: the signal pulses are frequency doubled in a 6.5-mm-long BBO crystal cut under 22.8° and the center wavelength of the generated second-harmonic light is determined with an optical multichannel analyzer (OMA) mounted on a spectrograph.

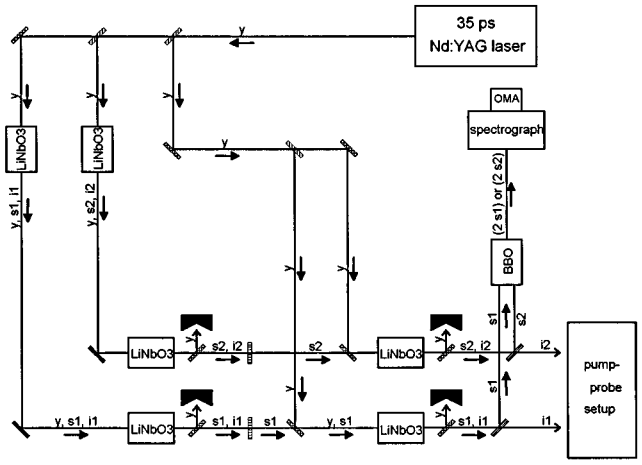

FIG. 1. Schematic representation of the experimental setup with which the picosecond mid-infrared laser pulses are generated. A single pulse from a mode-locked Nd:YAG laser, denoted by "y" in the figure, is split in several pulses which are used to pump two independently tunable mid-infrared generating laser branches, denoted by "1" and "2." Each branch consists of three $LiNbO_3$ nonlinear crystals in which parametric generation and amplification yields mid-infrared pulses at different frequencies, the signal "s" and the idler "i." The extra optical delays to accommodate temporal overlap of the pulses are not shown.

The idler pulses generated in this process have typical pulse energies of 100–200 μJ, depending on their exact frequencies, and have a pulse duration of 25 ps. The linewidths of the generated infrared pulses, which depend strongly on frequency, are determined using a scanning infrared spectrometer. It is found that at the O–D wavelengths, the spectral content of the pulses can be deduced directly from the second-harmonic spectrum of the doubled signal pulses. At the O–H wavelengths this is not possible, because the spectral widths are too large. The full spectral width at half maximum (FWHM) of the idler pulses ranges from about 7 cm^{-1} at the O–D absorption frequency to about 34 cm^{-1} at the O–H wavelength (see Table I for the experimental parameters), which means that the pulses are far from bandwidth limited.[53]

The independently tunable idler pulses are used to perform the pump–probe infrared saturation spectroscopy, for which the setup is depicted schematically in Fig. 2. One beam, i2 in Fig. 2, is focused onto the sample by a 100 mm CaF_2 lens. This is the pump pulse which excites a significant fraction of the vibrational oscillators and thereby saturates the absorption. From the other idler beam, i1 in Fig. 2, a low intensity pulse is split off by a thin CaF_2 plate which reflects about 1%. The transmitted high-intensity part (99%) of that pulse is stopped by a beam dump, and is not used in the two-color experiments. The reflected low-intensity pulse, which is the probe pulse, is sent into a variable delay (a gold-coated retroreflector on a translation stage) to vary the time delay with respect to the pump pulse. The probe pulse is focused onto the same spot of the sample as the pump pulse with the same 100 mm CaF_2 lens and is collimated with an-

TABLE I. Overview of some experimental parameters and results of the experiments discussed in Secs. IV A and IV B.

	O–D		O–H	
Quantity[a]	LF	HF	LF	HF
$\nu_{\text{center}}^{\text{abs}}$ (cm^{-1})	2620	2683	3549	3637
$\Delta\nu^{\text{abs}}$ (cm^{-1})	36	16	53	24
Occupation fraction[b]	56%	47%	100%	100%
ν_{anh} (cm^{-1})	92	86	172	162
$\Delta\nu_{0\rightarrow1}^{\text{las}}$ (cm^{-1})	5.8	8.1	33	35
$\Delta\nu_{1\rightarrow2}^{\text{las}}$ (cm^{-1})	4.8	6.4	30	12[c]
$\tau_{0\rightarrow1}$ (ps)	42±2	127±3	44±2	250±12
$\tau_{1\rightarrow2}$ (ps)	42±3	120±2	43±3	317±15[c]
$\delta\nu_{\text{hom}}$ (cm^{-1})	4±1[d]	4±1	≃5.4[e]	≃5.4[e]
T_1 (ps)	42±2	123±4	50–100	400–500
T_2^* (ps)	2.7±0.7[d]	2.7±0.7	≃2[e]	≃2[e]

[a]Properties of the absorption bands are denoted with "abs" and are obtained from the conventional infrared absorption spectrum. The spectral widths of the laser pulses (denoted with "las") depend strongly on wavelength and weakly on the alignment; the frequency (the transition to which the laser was tuned) is indicated as a subscript. All $\Delta\nu$ widths are FWHM.

[b]The percentage of oscillators which are studied D/(H+D) for the O–D experiments, H/(H+D) for the O–H experiments.

[c]At the red side of the $v_{1\rightarrow2}$ hot-band transition.

[d]Values of $\delta\nu_{\text{hom}}=7.0\pm1.5\ \text{cm}^{-1}$ and $T_2^* = 1.6 \pm 0.4$ ps are found in the low-frequency shoulder $\nu<2615\ \text{cm}^{-1}$.

[e]Inferred from the O–D results.

other 100 mm CaF_2 lens behind the sample. The transmitted probe energy is measured with a PbSe (signal) detector. A mechanical shutter is placed in the pump beam, which stops every second pump pulse, so that each pump–probe pulse pair is followed by a probe pulse only, to deduce the effect of the pump pulse on the transmission of the probe. To determine whether the detected transmitted probe pulse was accompanied by a pump pulse, the latter one is detected with another PbSe cell behind the sample as well (pump detector). To correct for pulse-to-pulse fluctuations of the probe intensity, before the sample a small part of the probe pulse is reflected out of the beam with another CaF_2 plate and its intensity is measured with a PbSe (reference) detector. Low-pass filters which only transmit the idler are placed in front of all detectors. The PbSe cells do not detect the infrared beams directly but, to reduce extra noise due to spatial fluctuations, are first diffused by roughened aluminum plates.[10] With this setup, the value of $\ln(T/T_0)$, where T is the transmitted probe energy in the presence of the exciting pump pulse and T_0 the probe transmission without the pump pulse, is determined.

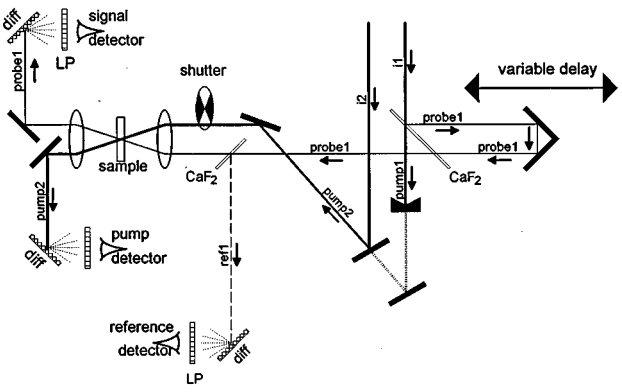

FIG. 2. Schematic representation of the experimental setup for time-resolved pump–probe spectroscopy. One of the idler beams generated with the setup depicted in Fig. 1, i2, is the pump beam. With a thin CaF_2 plate a weak part of the i1 beam is reflected and is sent into a variable delay, this pulse is the probe pulse. Pump and probe pulses are focused onto the same spot on the sample with the same CaF_2 lens and are collimated behind the sample with another lens. A reference probe pulse, the transmitted probe pulse, and the transmitted pump pulse are detected with PbSe detectors. Every other pump pulse is blocked with a beam shutter to record the probe transmission without the pump pulse. The diaphragms around the transmitted probe beam to suppress scattering of the pump beam by the zeolite sample are omitted in this graph.

The two-color saturation experiment allows for exploring a two-dimensional (time, frequency) parameter space and can be exploited in two ways:[5] the probe transmission can be measured (i) as a function of the time delay with respect to the pump by changing the variable delay or (ii) as a function of probe frequency at a fixed delay time with respect to the pump pulse. In the former experiment the dynamics of the excited level populations are monitored directly, whereas in the latter the transient absorption spectrum after excitation is recorded. The position of the variable delay is computer controlled and for all laser shots the position and the reading of all detectors is stored. A typical measurement as a function of time delay consists of 10 scans over 50 delay positions, and at each position 40 laser shots are collected (20 with pump, 20 without pump). To record the transient absorption spectrum at a fixed delay, typically 400 shots are collected per probe frequency. All experiments presented in this paper are performed at room temperature.

For an anharmonic molecular vibration, for which the level spacing changes with increasing energy in the vibra-

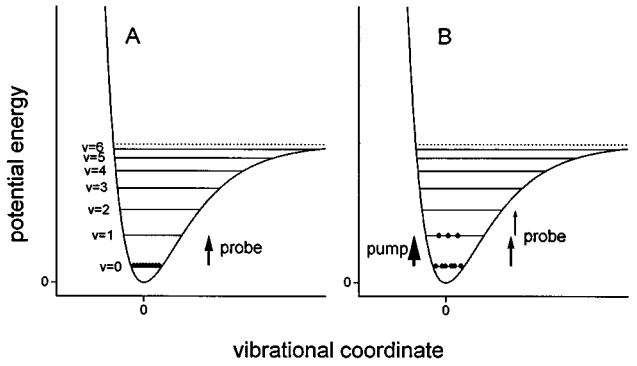

FIG. 3. Schematic representation of a vibrational potential and energy levels for a molecular vibration in the mid-infrared. The seven lowest energy levels are drawn as well as the dissociation energy (dotted line). The level spacing decreases with increasing energy due to the anharmonicity of the vibration. At room temperature in thermal equilibrium all vibrational population is in the $v=0$ ground state (A) and absorption occurs between $v=0$ and $v=1$. In pump–probe saturation spectroscopy a significant fraction of the population is excited to the $v=1$ excited state (B). As long as the $v=1$ state is populated, the absorption for a probe at the $v_{0\rightarrow1}$ transition is decreased and for a probe resonant with the $v_{1\rightarrow2}$ transition absorption to the $v=2$ level occurs.

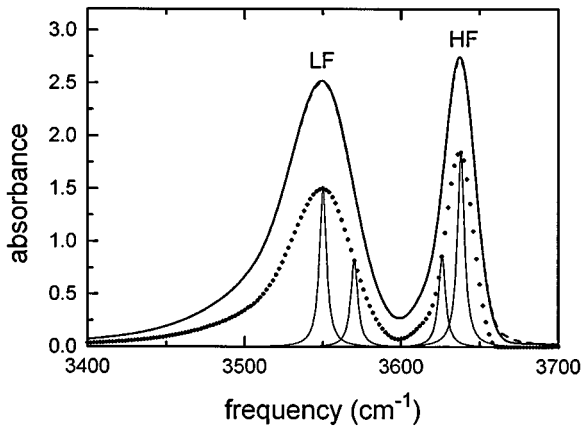

FIG. 4. Conventional infrared absorption spectra (thick solid line) for fully exchanged zeolite Y around the O–H stretch absorption frequency. The hydroxyl absorption spectrum displays two distinct absorption bands, one at lower frequency (LF) and one at higher frequency (HF). The spectrum has been decomposed in sets of equally spaced Lorentzians with FWHM widths of 5.4 cm^{-1}. The amplitudes for each Lorentzian are depicted with a dot and four Lorentzians are shown as examples (thin solid lines). When all the Lorentzians are summed (the amplitudes are scaled in this figure), the absorption spectrum which is depicted as the dashed line is obtained.

tional potential, the following signals for the probe transmission can be expected. For stretch vibrations in the mid-infrared at room temperature, without the saturating pump pulse, all the population is in the $v=0$ vibrational ground state, see Fig. 3(A). Hence, ignoring overtone absorption at higher frequencies, absorption only occurs between the $v=0$ ground state and the $v=1$ excited state. A strong pump pulse resonant with the fundamental $v_{0\rightarrow1}$ transition excites a significant fraction (in our experiments typically $\sim$10%–20%) of the oscillators to the first excited vibrational level, $v=1$ [see Fig. 3(B)]. Due to the anharmonicity of the molecular vibration, the pump is not resonant with the $v_{1\rightarrow2}$ transition. When the probe frequency is tuned to the same $v_{0\rightarrow1}$ transition, the transmission for the probe pulse is increased as long as it arrives simultaneously with or just after the exciting pump pulse due to a reduced population difference between the ground and excited state, implying that the fundamental absorption is ''bleached.'' As long as the $v=1$ level is populated, absorption from $v=1$ to $v=2$ can occur and consequently the transmission of a probe pulse at the $v_{1\rightarrow2}$ transition frequency is decreased. This induced absorption band between the first and second excited levels is referred to as the ''hot band'' and is located at a somewhat smaller frequency than the fundamental transition due to the anharmonicity of the vibration. By varying the time delay of the probe pulse with respect to the pump pulse, the return to equilibrium for both transitions can be monitored.

B. Samples

Zeolites are alumino-silicates and form very porous crystalline frameworks. The charge compensation, needed for every silicon atom replaced by an aluminum atom, is provided by Na^+ cations in the interstices of the structure. The proton loaded zeolites which we have investigated here were obtained by heating *in vacuo* (at least 1 h at 723 K) zeolites in which the Na^+ cations were exchanged for NH_4^+ cations. (The samples were self-supported discs of 4–6 mg/cm^2).[54,55] All experiments were done at room temperature with the samples *in vacuo* and were performed within two days after heating to prevent water contamination.

We have studied proton-loaded zeolites Y with a silicon to aluminum ratio of Si/Al=2.8. Zeolite Y is known to have a faujasite structure[56] and in the exchanged versions the acid protons are covalently bonded to oxygen atoms around aluminum atoms. The protons are found on three of the four crystallographically different oxygen sites in the structure.[57] The absorption spectra around the O–H stretch frequency as measured with a conventional infrared absorption spectrometer is depicted in Fig. 4. Two absorption bands, one at higher frequency (HF) and one at lower frequency (LF) are distinguished. The LF absorption band arises from protons which point into the smaller sodalite cages[57] and form weak hydrogen bonds with nearby oxygen atoms in the structure.[38] The HF absorption band arises from hydroxyls pointing into the larger supercages of the structure.

Besides the dynamics of the O–H vibration, we also studied the O–D vibrations in the same zeolites with time-resolved saturation spectroscopy. The deuterated versions of the acid zeolites were obtained by keeping the samples for some time (a few hours to one day typically) at an elevated temperature (between room temperature and 723 K) in a background of D_2 gas, after the standard bakeout procedure. As can be inferred from the conventional O–D absorption spectrum (see, e.g., Fig. 5) the protons which constitute the two absorption bands are exchanged for deuterons at the same level. Depending on the temperature, time, and background pressure of the D_2 gas during the deuteration process, different levels of exchange (up to 80%) could be attained.

The ratio of O–H vs O–D is inferred from the infrared absorption spectra.

III. SIMULATION OF THE TRANSIENTS

A straightforward calculation of the transient changes in transmission as a function of the time delay between pump and probe pulses is performed by solving the differential equations in which the time dependence of the laser pulses and an exponential decay time for the transmission change are taken into account. In this calculation the transmission changes proportionally to the time-integrated pump intensity and relaxes with a single exponential decay time τ. With this calculation we will extract single exponential decay times τ from all probe transmission signals as a function of the time-delay t. This is done by fitting τ to the experimental data, where the probe transmission is allowed to decay to a different but constant level (also a fit parameter). The error in the decay time is the standard deviation in τ as obtained by this procedure. The rate-equation calculation of the full transient signal allows for a determination of the position of the time delay where pump and probe pulses have exact temporal overlap, i.e., $t=0$.

It is tempting to interpret the transient-transmission decay time τ as the vibrational lifetime T_1 of the investigated excited level, but great care has to be taken (see also the appendix of Ref. 15). First of all, the lifetime of the population difference between $v=1$ and $v=0$ and the lifetime of the $v=1$ excited state need not to be the same, because the $v=1$ population may decay to other intermediate levels before relaxing to the $v=0$ ground state. The existence of such intermediate levels can be explored by comparing the results of one-color pump–probe experiments, which reveal the decay time for the excited population difference, to the results of two-color experiments where the population decay of the $v=1$ level is directly monitored by a probe at the $v_{1\rightarrow 2}$ hot-band frequency. Second, in the case of non-negligible excitation of the oscillators by the pump pulse, the exponential decay time τ as determined for the transmission changes may differ from the relevant population lifetime T_1. In Appendix A it is shown that the occurrence of different fractions of excitations within the probe bandwidth may lead to transmission decay times that differ from the population lifetime.

The absorption bands in zeolites are expected to be inhomogeneously broadened due to the random distribution of Al atoms in the lattice as well as due to lattice imperfections. In a previous study[38] we found that the population decay time for the O–H stretch vibration varies over the LF absorption band, due to a distribution of hydrogen bond strengths, which indeed shows that the homogeneous linewidth is smaller than the absorption band. In experiments in which the transient absorption spectrum is recorded by tuning the probe frequency information about the homogeneous linewidth can be obtained.

To simulate the transient signals and compare them with our data, the absorption spectra of the zeolites are decomposed into sets of homogeneous Lorentzian lines. The inhomogeneous absorption spectrum is deconvoluted with a Lorentzian of a certain, adjustable, width $\delta\nu_{\mathrm{hom}}$. This $\delta\nu_{\mathrm{hom}}$ is used as a fit parameter. The deconvolution is performed by inverse Fourier transformation of the ratio of the Fourier transforms of the inhomogeneous spectrum and the Lorentzian line. This yields the amplitudes a_i of the Lorentzians which, when added together, compose the following inhomogeneous absorption spectrum:

$$A(\nu)=\sum_i L_i(\nu)=\sum_i \frac{a_i}{\pi}\frac{\frac{1}{2}\delta\nu_{\mathrm{hom}}}{(\nu-\nu_{\mathrm{hom},i})^2+(\frac{1}{2}\delta\nu_{\mathrm{hom}})^2}, \tag{1}$$

where $\nu_{\mathrm{hom},i}$ is the center frequency of the ith homogeneous Lorentzian line. For a correct description, the spacing between the Lorentzians should be smaller than the FWHM linewidth $\delta\nu_{\mathrm{hom}}$. An example of this decomposition procedure is shown in Fig. 4. The O–H inhomogeneous absorption spectrum, measured with a conventional infrared absorption spectrometer, is decomposed into sets of homogeneous lines having a FWHM width of $\delta\nu_{\mathrm{hom}}=5.4\ \mathrm{cm}^{-1}$.

Using the deconvolution method described above, the *homogeneous* linewidths can be determined from the transient absorption spectra as follows. If saturation of the absorption is neglected, the initial excitation fraction $\mathscr{F}_i$ for each homogeneous Lorentzian line $L_i(\nu)$, can be approximated to be proportional to the pump energy, spectrally integrated over the homogeneous band,

$$\mathscr{F}_i=\chi\int T_{\mathrm{pu}}(\nu)L_i(\nu)\,d\nu, \tag{2}$$

where $T_{\mathrm{pu}}(\nu)$ is the pump spectrum and χ is a proportionality constant. Here the time-dependent pump intensity is integrated out, $\int I_{\mathrm{pu}}(t)dt=T_{\mathrm{pu}}$, because we are interested in the excited spectrum just after the pump pulse. Due to saturation of the homogeneous lines which are excited with the largest laser intensities (at the center of the laser spectrum), however, the excited fractions of these lines will be somewhat smaller than expected from Eq. (2). If saturation of the absorption is taken into account, the time-dependent excited fractions $f_i(t)$ change during the pump pulse as $\partial f_i/\partial t=(1-2f_i)I_{\mathrm{pu}}(t)$. If the time integration is now performed, the initial excited fraction for each homogeneous Lorentzian line after the bleaching pump pulse is calculated as

$$f_{e,i}=\frac{1-\exp(-2\mathscr{F}_i)}{2}, \tag{3}$$

with $\mathscr{F}_i$ given by Eq. (2). The constant χ is adapted to yield the same initial signal as in the experiments. In the description given by Eqs. (2) and (3) the depth dependence of the excitation is integrated out. The assumption of an effective, constant, population difference for the pump intensity, neglects that at very large saturation levels the bleaching of the homogeneous lines at different frequencies will mutually influence each other. This is neglected here because this effect is expected to be small at the saturation levels used in our experiments. However, saturation of the homogeneous lines

is explicitly taken into account in Eq. (3) and thus there is accounted for power broadening[58] by the pump in our description of the excited spectrum.

To account for the population decay of the excitations with a lifetime T_1, the time dependence for the excited fraction per homogeneous band is given by

$$f_i(t) = f_{e,i} \exp\left(-\frac{t}{T_1}\right). \tag{4}$$

The transient absorbance at the fundamental transition as a function of frequency and delay time t is given by

$$A_{0\to1}(\nu,t) = \sum_i [1-2f_i(t)]L_i(\nu). \tag{5}$$

The population which is excited to $v=1$ absorbs at the hot-band frequency $v_{1\to2}$, which is a ν_{anh} smaller than the fundamental $v_{0\to1}$ transition frequency due to anharmonicity. The induced absorbance at the hot-band transition reads as follows:

$$A_{1\to2}(\nu,t) = \sum_i \beta f_i(t) L_i(\nu+\nu_{\text{anh}}), \tag{6}$$

where β is a parameter which scales the $v_{0\to1}$ absorption cross section to the $v_{1\to2}$ absorption cross section ($\beta=2$ for a harmonic oscillator). The transient absorbance spectrum is given by the sum of Eqs. (5) and (6), $A(\nu,t)=A_{0\to1}(\nu,t)+A_{1\to2}(\nu,t)$. To compare this time-dependent absorbance with the transient data, the probe transmission as a function of both central probe frequency and delay time has to be calculated,

$$T(\nu_{\text{pro}},t) = \int T_{\text{pro}}(\nu)\exp[-A(\nu,t)]d\nu, \tag{7}$$

where $T_{\text{pro}}(\nu)$ is the probe spectrum with a center frequency of ν_{pro}. The probe transmission $\ln(T/T_0)$ as a function of probe frequency is calculated according to the procedure described above for several values of the homogeneous linewidth $\delta\nu_{\text{hom}}$. By comparing the calculated spectra with the measured transient spectra the value for the homogeneous linewidth is obtained.

IV. RESULTS AND DISCUSSION

A. Vibrational dynamics of O–D: T_1 lifetimes and homogeneous linewidths

At the O–D wavelength our laser pulses have a much smaller spectral width than at the O–H wavelengths, which results in a better signal-to-noise ratio and an improved frequency resolution[42] (see Table I for an overview of the experimental parameters and the results). Furthermore, we will show later that for the O–D experiments spectral diffusion is negligible (due to lower concentrations of oscillators and smaller transition dipole moments compared to the O–H vibrations). This allows for a straightforward interpretation of the O–D transient signals in terms of population decay and pure dephasing.

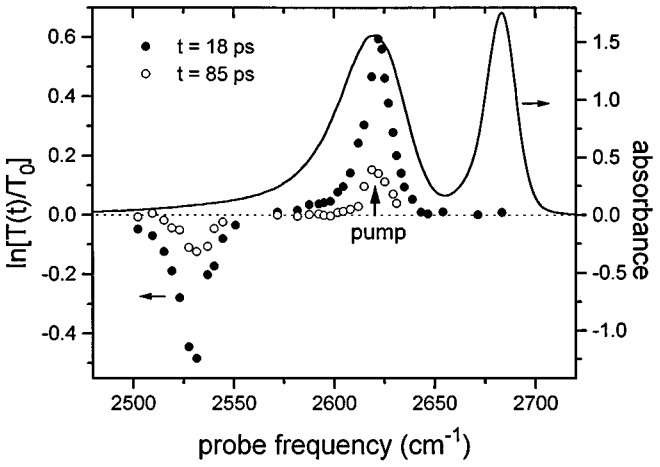

FIG. 5. Transient transmission spectrum after excitation of the LF O–D stretch vibration (dots), measured by tuning the probe frequency, and the conventional absorption spectrum (line). The transient spectrum is plotted for two delay times t with respect to the saturating pump pulse. At the pump frequency the transmission is increased due to bleaching of the fundamental transition, and at a lower frequency the excited state hot-band absorption appears (see also Fig. 3). Note that the spectral width of the bleaching around the pump frequency is smaller than the LF absorption band, which means that a transient spectral hole is burnt.

A transient transmission spectrum just after excitation by a pump pulse at the LF absorption frequency is presented in Fig. 5 (for reference, the conventional absorption spectrum measured by an infrared absorption spectrometer is depicted as well). At a time delay of $t=18$ ps, after exact temporal overlap between pump and probe pulses, two spectral features are recorded by tuning the probe frequency (see also Fig. 3). First, around the pump frequency, the absorption is bleached and second, a transient hot band is observed at 2529 cm^{-1}. From the frequency difference between the bleaching of the fundamental band and the induced $v_{1\to2}$ hot band an anharmonicity of 92 cm^{-1} between the first two transitions is determined. It should be noted that the width of the bleaching is much smaller than the absorption linewidth. Apparently the pump pulse only excites a subset of different oscillators within the absorption band and other oscillators within the band remain unaffected. This means that a transient spectral hole is burnt,[9,31,32] which reveals that the absorption band was formed by a distribution of different vibrational frequencies (as anticipated in Sec. III), i.e., the band is inhomogeneously broadened. This explicitly proves the inhomogeneity of the hydroxyl sites, which is an important issue in present zeolite research.[59–63]

At a later delay time of 85 ps, both the bleaching of the fundamental band and the absorption at the hot-band frequency have decreased in amplitude due to the population decay of the $v=1$ excited state. Because the LF oscillators are hydrogen bonded, the T_1 lifetimes decrease with decreasing frequencies in the LF absorption band[38] and therefore the bleaching line shape changes with delay time. To monitor the dynamics of the vibrational relaxation at the top of the LF absorption band, the probe frequency is fixed and the probe transmission is recorded as a function of the delay with re-

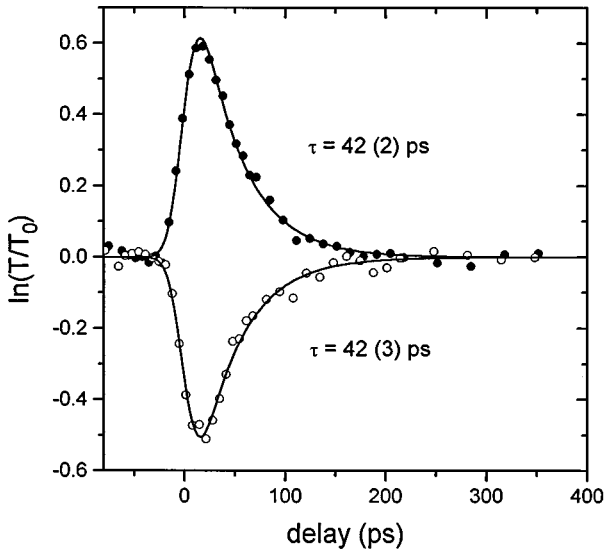

FIG. 6. Transmission change of a probe pulse as a function of delay time with a pump pulse which excites the LF O–D vibration at $t=0$ (see Fig. 5). The filled dots are measured with a probe frequency at the fundamental LF absorption at 2622 cm^{-1} and show an increase of the probe transmission, due to bleaching of the transition by the pump pulse. The open dots represent the probe transmission at the hot-band frequency of 2530 cm^{-1}. The solid lines are calculated transients for which a single exponential decay time τ (indicated in the graph) is assumed for the transmission change (see Sec. III).

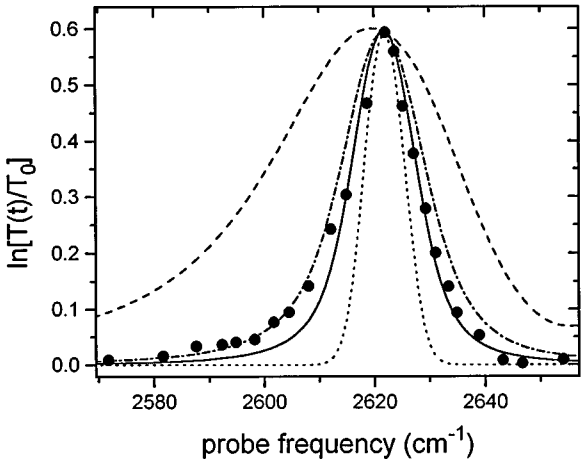

FIG. 7. The transient spectral hole for the LF O–D absorption at delay $t=18$ ps (●) compared to several spectra. The dotted line represents the instrumental function, determined by the linewidths of pump and probe pulses. The unexcited inhomogeneous absorption band convoluted with the probe spectrum is represented by the dashed line. The experimental data are in between these extremes. The main part of the spectral hole can be described well if the inhomogeneous spectrum is decomposed (see Sec. III) into homogeneous lines with a linewidth of $\delta\nu_{\mathrm{hom}}=4$ cm^{-1} (solid line), but the data at the smallest frequencies ($\nu<2615$ cm^{-1}) suggest a larger linewidth of $\delta\nu_{\mathrm{hom}}=7$ cm^{-1} in the low-frequency shoulder of the absorption band (dash–dotted line).

spect to the pump. In Fig. 6 the time-dependent transmission changes for the probe at the top of the fundamental absorption band (frequency the same as the pump frequency) and for the probe at the top of the hot-band frequency are shown. The delay $t=0$ ps corresponds to the exact temporal overlap between pump and probe pulses. At the fundamental absorption frequency an increase of the transmission upon excitation is observed which decays with an exponential decay time of $\tau=42\pm2$ ps (see Sec. III for the calculation of the solid line). At the $\upsilon_{1\rightarrow2}$ hot-band frequency a decrease in transmission is found which relaxes with an identical time constant of $\tau=42\pm3$ ps to the original value. Because the bleaching and hot-band lifetimes are equal it is inferred that relaxation from the $\upsilon=1$ state occurs directly to the $\upsilon=0$ ground state and that no other intermediate levels are involved. Taking into account the effects discussed in Appendix A, we may identify the decay time of the transmission changes as the population decay time for the $\upsilon=1$ excited level for the center of the LF O–D absorption band: $T_1(\nu\simeq2620\ cm^{-1})=42$ ps.

From the width of the spectral hole (Fig. 5) and the laser linewidth, the width of the homogeneous lines which constitute the inhomogeneous absorption band can be determined, using the procedure described in Sec. III. In Fig. 7 the experimental bleaching at $t=18$ ps is compared to calculations of transmitted probe spectra. The measured spectral hole is much smaller than the full inhomogeneous absorption band as measured by the probe pulses (dashed line) and broader than the instrumental function (dotted line). The main part of the measured spectral hole is described well by the simulations if a FWHM bandwidth of $\delta\nu_{\mathrm{hom}}=4\pm1$ cm^{-1} for the homogeneous lines is assumed. At the lowest frequencies in the LF band however, the data suggest that the homogeneous bandwidth is broader, and from the calculations we estimate $\delta\nu_{\mathrm{hom}}=7.0\pm1.5$ cm^{-1} for that low-frequency shoulder (dash–dotted line). The homogeneous linewidth is determined by the population lifetime T_1 and by the pure dephasing time T_2^* as $\delta\nu_{\mathrm{hom}}=(2\pi T_1)^{-1}+(\pi T_2^*)^{-1}$. Taking the measured population lifetime for the top of the LF band into account (see Fig. 6), $T_1=42$ ps, these homogeneous bandwidths yield the following values for the pure dephasing time: $T_2^*=2.7\pm0.7$ ps for $\nu>2615$ cm^{-1} and $T_2^*=1.6\pm0.4$ ps at smaller frequencies in the LF O–D absorption band.[64] From the observation that the main part of the LF absorption band can be described with a single value for the dephasing time, it is inferred that T_2^* is less affected by H bonding than the T_1 lifetime, which strongly varies over the whole absorption band.[38] Apparently only for the strongest *H*-bonded oscillators (at the lowest absorption frequencies) is T_2^* also reduced.

To investigate the vibrational dynamics of the HF oscillators, the pump frequency is tuned to the HF absorption band, at 2684 cm^{-1}. From the transient spectrum an anharmonicity of 85 cm^{-1} is determined between the fundamental and the hot-band absorption. The somewhat larger anharmonicity for the LF vibration as compared with the HF vibration is expected because hydrogen bonding of the LF oscillators increases the anharmonicity.[38] To monitor the dynamics of the spectral changes, the transmission of the probe is again recorded as a function of delay with the pump,

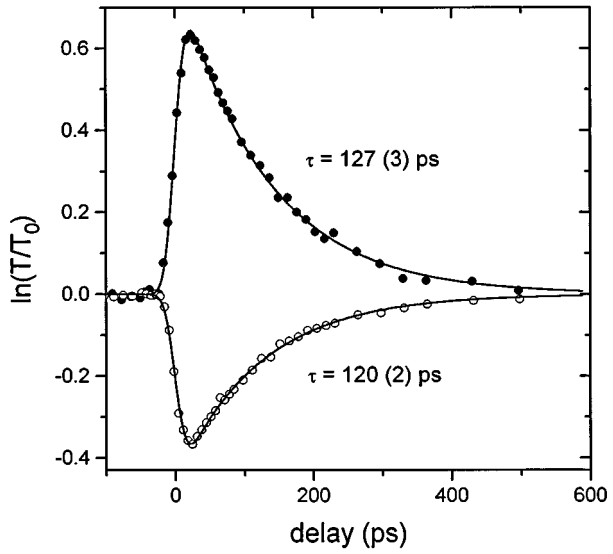

FIG. 8. Transmission change of a probe pulse at the fundamental absorption (2684 cm^{-1}, ●) and at the induced hot-band transition (2599 cm^{-1}, ○), for excitation at the HF O–D absorption by a pump pulse at $t=0$, as a function of delay time. The single exponential decay times (and standard deviations) of both transmission changes are indicated in the graph.

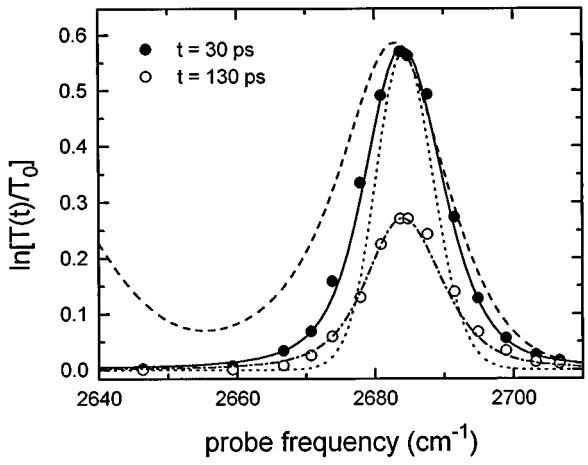

FIG. 9. The same as in Fig. 7 for the measured transient spectral hole in the HF O–D absorption band for delay $t=30$ ps (●) and $t=130$ ps (○), compared to several spectra. The experimental data at $t=30$ ps (●) are in between the instrumental function (dotted line) and the inhomogeneous absorption spectrum as measured by the probe (dashed line). The experimental data are described well with $\delta\nu_{\mathrm{hom}}=4$ cm^{-1} (solid line), using the deconvolution procedure of Sec. III. The spectral hole has decreased in amplitude 100 ps later (○), which is well described by the same calculation that yielded the solid line, using the exponential decay time for the excitations determined in Fig. 8 (dash–dotted curve).

for the probe frequency fixed at the fundamental absorption and for the probe resonant with the induced absorption hot band. These transient transmission changes are shown in Fig. 8 and similar decay times of $\tau\simeq 123$ ps are determined for both transients. Again this time may be interpreted as the population decay time T_1 for the excited $v=1$ level of the HF O–D vibration. The longer T_1 lifetime for the HF vibration than for the LF vibration at the O–D wavelength is consistent with our previous results of single-color experiments on the O–H vibrations.[38] Due to hydrogen bonding of the LF oscillators the relaxation rate is increased compared to the HF oscillators.

The spectral hole for the HF O–D vibrations is plotted in Fig. 9 for two delay times with respect to the pump, to again extract the homogeneous linewidths (analogous to Fig. 7). In Fig. 9 the experimental data are compared to calculations of transmitted probe spectra (see Sec. III). The measured spectral hole is clearly smaller than the full inhomogeneous absorption band as measured by the probe pulses and broader than the instrumental function. The calculated transient spectrum agrees well with the experimental data for a constant homogeneous FWHM bandwidth of $\delta\nu_{\mathrm{hom}}=4\pm 1$ cm^{-1}. The dash-dotted line in Fig. 9 is given by the same simulation as the solid line, with the excited fractions scaled by a factor $\exp(-t/\tau)$ [see Eq. (4)] with $t=100$ ps and $\tau=123$ ps (see Fig. 8). This simulation agrees well with the experimental data represented by the open dots in Fig. 9. Thus we find that the shape of the hole remains the same during vibrational relaxation, which implies that there is no spectral diffusion. This confirms that the transient spectroscopic data can indeed be interpreted in terms of population decay and homogeneous broadening. Combining the homogeneous linewidth and the T_1 lifetime determined from Fig. 8, the pure dephasing time T_2^* for the HF O–D vibration is determined to be 2.7 ± 0.7 ps.

B. Vibrational dynamics of O–H: Spectral diffusion

In comparison with the O–D experiments described in Sec. IV A, the time-resolved experiments on the O–H oscillators are different in several aspects. First of all, at the O–H wavelength the linewidth of our laser pulses is larger than at the O–D wavelength (see Table I), which decreases the spectral resolution and makes the effect of spectral averaging of the transmitted probe (see Appendix A) more important. Furthermore, the transition dipole moments of the O–H vibrations are larger than for the O–D vibrations (the ratio between the absorption cross sections is $\sigma_{\mathrm{OD}}/\sigma_{\mathrm{OH}}=0.7$) and also the concentration of oscillators in the pure O–H samples is higher than in the deuterated O–D samples. This results in the occurrence of spectral diffusion during the vibrational relaxation process as we will show in this section.

First we consider the experiments on the LF O–H vibration. With the pump at the center of the absorption band, a spectral hole was burnt into the LF band: the LF absorption band as measured by the spectrally broad laser pulses has a FWHM width of 61 cm^{-1}, whereas for the bleaching FWHM $\sim$42 cm^{-1}. The anharmonicity was determined to be 172 cm^{-1} and for both the bleaching and for the induced hot-band absorption an exponential decay time of $\tau\simeq 44$ ps is found.

The spectral changes just after excitation of the HF oscillators are shown in Fig. 10. The width of the bleaching around the pump frequency corresponds to the width of the inhomogeneous absorption band convoluted with the laser

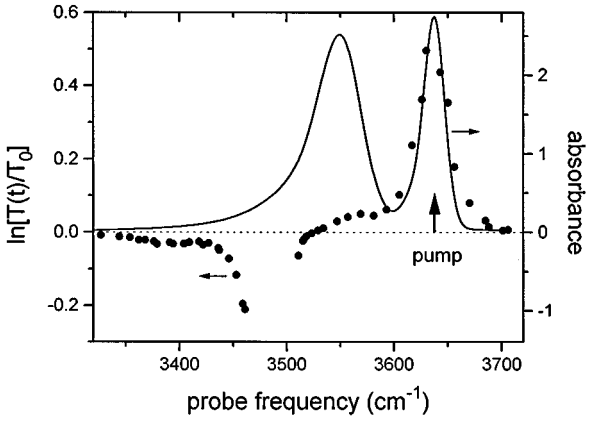

FIG. 10. Transient transmission spectra (●) for a probe pulse 32 ps after excitation of the HF O–H vibration by a saturating pump pulse at 3638 cm^{-1} (the conventional absorption spectrum is depicted as the solid line for reference). The HF absorption band is bleached and an induced hot-band absorption is found around 3476 cm^{-1}. The top of the induced hot band cannot be recorded because, due absorption of water in the $LiNbO_3$ crystals (Fig. 1), no light can be generated in the region of 3465–3510 cm^{-1}.

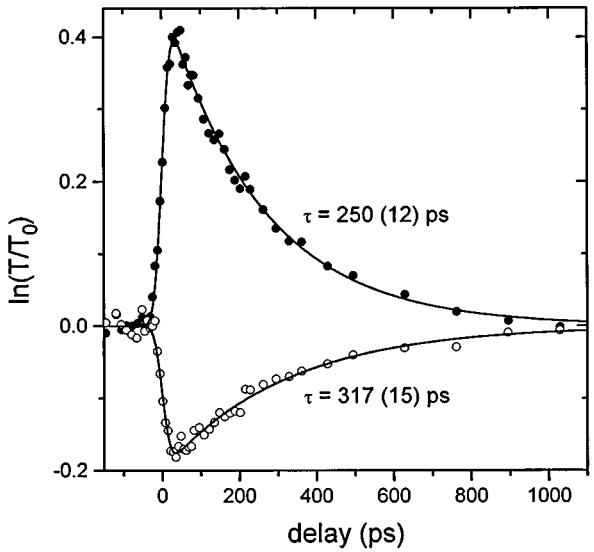

FIG. 11. Probe transmission change as a function of delay time with a saturating pump pulse at the HF O–H absorption. For the probe frequency resonant with the fundamental $v_{0\rightarrow1}$ absorption (3638 cm^{-1}, ●) the induced bleaching is found to decay with a single exponential time constant of 250±12 ps. The induced hot-band absorption, probed at the red side of the hot band (3459 cm^{-1}, ○), has a lifetime of 317±15 ps.

spectrum, because the laser spectrum is too broad compared to the absorption band to burn a hole. Due to water absorption in the $LiNbO_3$ crystals used for the generation of the infrared laser pulses (see Sec. II), no light can be generated in the region of 3465–3510 cm^{-1}. This prevents us from recording the top of the induced hot-band absorption. Nevertheless, from the wings of the hot-band absorption the peak position can be estimated, and from this an anharmonicity between the first and second transition of 162 cm^{-1} is determined. The values which we obtain for the anharmonicities between the first two transitions are in agreement with the results obtained from overtone spectroscopy.[65] The induced bleaching decays with an exponential time constant of $\tau=250$ ps if the probe is tuned to the same frequency as the pump, as is shown in Fig. 11. Due to the opaque window in our laser system, the probe is tuned to the red side of the induced hot band, to 3459 cm^{-1}, to monitor the hot-band dynamics. At that frequency, the induced absorption decays exponentially with a time constant of $\tau=317$ ps (Fig. 11). This is surprising, because for the first time we find different lifetimes for the induced changes in transmission at the fundamental and the hot-band frequencies (see Table I).

At 3459 cm^{-1}, the laser spectrum is just at the edge of the water absorption in the $LiNbO_3$ crystals. This causes a narrowing of the laser linewidth to FWHM=12 cm^{-1}. Thus, with this probe frequency at the red side of the induced HF hot band, a different (spectrally narrow) subset of oscillators is monitored than in the experiment in which the probe frequency is equal to the pump frequency. To check whether the longer lifetime for the hot-band absorption compared to the lifetime for the bleaching (Fig. 11) is due to the probing of different subsets of oscillators, we performed the following experiment. The probe frequency is fixed to 3459 cm^{-1}, so that the spectral changes at the $v_{1\rightarrow2}$ transition are recorded for a spectrally narrow subset of HF oscillators which have the lowest frequencies within the HF absorption band.[66] The transmission of the probe as a function of the delay is now measured for two different *pump* frequencies, see Fig. 12. We find that the lifetime of the hot-band absorption is significantly shorter for the center of the pump bandwidth at the red side of the fundamental band than for excitation at the blue side of the band. The transient absorption lifetimes τ for several values of the center frequency of the pump are plotted in Fig. 13. The transient absorption probed at the red side

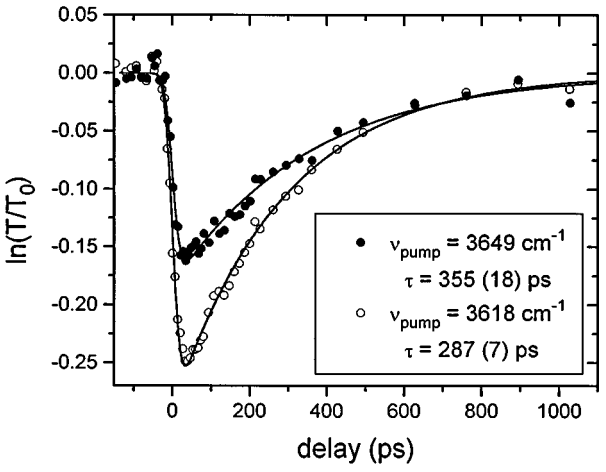

FIG. 12. Probe transmission change at the red side of the induced hot band (probe frequency=3459 cm^{-1}) as a function of the delay time with respect to the pump pulse, for two different pump frequencies (indicated in the graph). The lifetime of the induced transient absorption is significantly increased when the excitation frequency is tuned from the red side of the fundamental absorption band (○) to the blue side of the fundamental band (●).

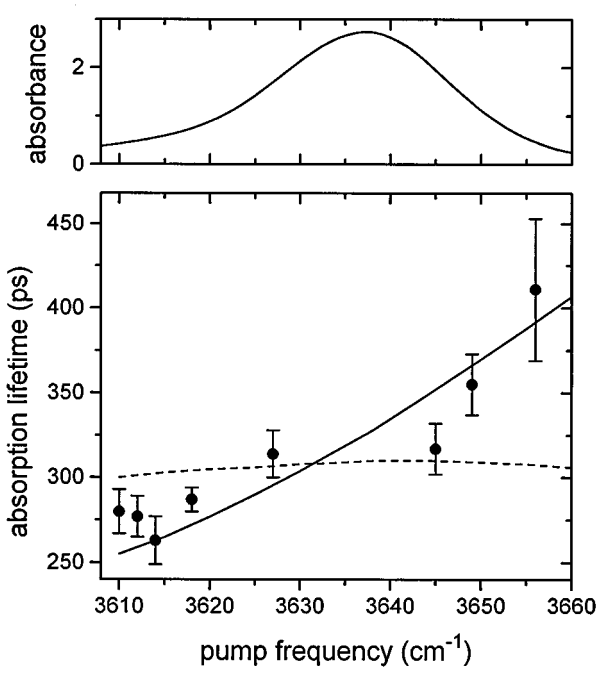

FIG. 13. Lower panel: transient absorption lifetime (●, see Fig. 12) for a probe pulse with its central frequency fixed at the red side of the $v_{1\rightarrow 2}$ hot band (at 3459 cm^{-1}), as a function of the central frequency of the exciting pump pulse. The probe pulse monitors the population in the excited $v=1$ level for a subset of oscillators with fundamental absorption frequencies around 3621 cm^{-1} (=3459 cm^{-1}+anharmonicity). The dashed curve results from a calculation of the spectral changes, assuming a homogeneous linewidth of $\delta\nu_{\mathrm{hom}}=5.4$ cm^{-1} and a fixed T_1 lifetime of 300 ps over the whole HF absorption band, for which all spectral averaging effects (Appendix A) are taken into account. The solid curve is the result of a simulation of the transient spectral changes in the presence of Förster energy transfer (see Sec. IV C). For reference, the conventional absorption spectrum is plotted in the upper panel.

of the hot band clearly lives longer after excitation at the blue side than after excitation at the red side of the absorption band.

The results of Fig. 13 are interpreted as spectral diffusion of the vibrational excitations. Before doing so, other possible effects which might cause a dependence of the hot-band lifetime on the pump frequency are considered. Although in all experiments in Fig. 13 the same subset of oscillators is probed, the increasing transient absorption lifetime τ with increasing pump frequency could in principle be due to different distributions of excitations within the probe linewidth (see also Appendix A). To check this, we have simulated the probe transmission as a function of delay for different pump frequencies using Eqs. (5)–(7) and the O–H absorption spectrum deconvoluted in Lorentzian homogeneous lines with FWHM=5.4 cm^{-1} (see Fig. 4). This value is obtained by scaling the average value that we found for the homogeneous linewidth in the O–D experiments with the ratio of O–H and O–D absorption frequencies.[67] If a constant T_1 lifetime is assumed for all the oscillators in the HF absorption band, the simulation gives a dependence of the absorption lifetime on pump frequency as shown by the dashed curve in Fig. 13. This dashed curve contains all spectral averaging effects discussed in Appendix A and it is clear that these effects cannot explain the observed dependence of the absorption lifetime on pump frequency. Better agreement between the experimental data of Fig. 13 with the simulations is obtained if the T_1 would increase from 190 ps at 3615 cm^{-1} to 610 ps at 3650 cm^{-1}.[68] However, the same simulation shows that this large increase in T_1 population lifetimes with frequency should also result in a strong dependence of the transient bleaching lifetime on the laser frequency in a one-color experiment: the observed decay should vary by a factor 2 if the pulses are tuned from 3615 to 3650 cm^{-1}. However, we did not find such a strong dependence of the bleaching lifetime on the laser frequency for the HF absorption band.[38] In fact, by tuning our laser pulses over the HF absorption band, the measured decay time for the one-color transient transmission was found to be within ±10% of the average value when the laser frequency was tuned over 30 cm^{-1} around the absorption maximum (see also Ref. 41). Furthermore, such a dependence would give rise to a much larger lifetime τ of the bleaching at the maximum of the absorption band in a one-color experiment than the lifetime of the induced absorption at the red side of the hot band. However, the contrary is observed, see Fig. 11. Thus we conclude that the results presented in Fig. 13 can result neither from a frequency dependence of the population lifetime T_1 in the HF absorption band nor from the spectral averaging over the probe spectrum (see Appendix A).

The observed dependence of the transient absorption lifetime on pump frequency can only be explained by spectral diffusion of the excitations. For all pump frequencies of Fig. 13 the probe has spectral overlap with (at least part of) the $v_{1\rightarrow 2}$ hot-band absorption of the excited oscillators. Therefore, for all pump frequencies there is an immediate induced absorption upon excitation. The *lifetime* of the induced hot-band absorption, reflecting the excited population of the subset of probed oscillators, is determined by two effects: (i) vibrational relaxation of the O–H stretch vibrations and (ii) direct transfer of excitations to or from other oscillators at other frequencies within the inhomogeneous absorption spectrum. For the pump frequency *resonant* with the frequency of the probed oscillators, at the red side of the absorption band, excitations are transferred to oscillators with other frequencies, which are not probed. Spectral diffusion of the excitations then acts as a depopulation channel for the excited level of the probed oscillators, additional to vibrational relaxation, and consequently the transient absorption lifetime is shortened. In the case of slightly *off-resonant* excitation, at the blue side of the absorption band, excitations are transferred from oscillators at the pump frequency to the probed oscillators at the red side. In this way the $v=1$ excited level of the probed oscillators is being populated *after* excitation by the pump pulse and consequently the observed transient absorption lives longer than expected from the vibrational relaxation time T_1 alone. In Sec. IV C it will be shown that this spectral diffusion is likely caused by dipole–dipole coupling of the vibrational excitations.

TABLE II. Structural information of the possible oscillator sites of the faujasite structure of zeolite Y (based on the structural information of Ref. 57). Protons are found in fully exchanged zeolite Y on O_1, O_2, and O_3 oxygen sites. For each of these sites, the distance R and orientation factor κ^2 is calculated, for the nearest dipole sites within a radius of 6 Å. With a number (1, 2, or 3) the kind of oxygen site is denoted (O_1–H_1, O_2–H_2, and O_3–H_3), and # denotes the number of identical sites. Note that there are the *possible* sites and that the protons in the lattice are distributed over these sites.

O_1–H_1				O_2–H_2				O_3–H_3			
Site	R (Å)	κ^2	#	Site	R (Å)	κ^2	#	Site	R (Å)	κ^2	#
2	3.2	1.43	2	3	2.9	0.06	2	3	2.8	2.99	2
3	3.3	0.67	2	2	3	2.88	2	2	2.9	0.06	2
2	3.4	0.62	2	2	3	0.51	1	1	3.3	0.67	2
2	3.4	0.00	2	2	3.1	0.11	1	3	3.7	0.23	2
3	3.7	1.76	2	2	3.1	0.02	2	3	4.2	1.41	1
1	4.2	1.56	2	1	3.2	1.43	2	2	4.3	0.67	1
1	4.6	1.56	2	2	4.3	0.14	1	3	4.6	0.00	1
3	4.8	0.55	2	3	4.3	0.67	1	2	4.6	0.11	2
2	4.9	0.33	2	3	4.6	0.11	2	1	4.8	0.55	2
2	4.9	0.09	2	1	4.9	0.09	2	2	4.9	1.89	1
3	5.2	0.03	2	3	4.9	1.89	1	2	5.2	0.88	1
3	5.5	0.02	2	3	5.2	0.83	2	2	5.2	0.55	1
3	5.6	0.18	2	3	5.4	0.09	2	2	5.4	0.09	2
2	5.8	2.02	2	3	5.4	0.09	2	2	5.4	0.39	1
3	5.9	2.32	2	2	5.6	1.55	2	1	5.5	0.02	2
				2	5.6	1.55	2	1	5.9	2.32	2
				1	5.8	2.02	2	2	5.9	1.19	2
				2	5.8	2.57	2	2	6.0	0.09	1
				3	5.9	1.19	2				
				3	6.0	0.02	1				

C. Direct energy transfer

The results in Fig. 13 show that the excited state population at the red side of the absorption band lives longer when most of the excitations are initially at the blue side of the band. Due to spectral migration of the excitations, the excited state of the probed oscillators is populated continuously after excitation and is therefore perceived to live longer. Because the O–H oscillators are fixed within the zeolitic lattice, their (inhomogeneously distributed) frequencies remain the same, and spectral diffusion of the vibrational excitations can only occur by transfer of the excitations between different O–H sites with slightly different frequencies. Dipole–dipole interactions between the oscillators can lead to site-to-site energy transfer of excitations. This is the so-called Förster transfer,[69] which is well known for electronic systems,[46–48] and has recently also been observed for vibrations on a surface.[24,25]

The Förster transfer rate from an excited donor dipole to an unexcited acceptor dipole is given by[69]

$$k_{d\to a}=\frac{\kappa^2\mu_d^2\mu_a^2}{4n^4\epsilon_0^2h^2cR^6}\int_0^\infty g_d(\nu)g_a(\nu)d\nu, \tag{8}$$

where μ_d and μ_a are the transition dipole moments of the donor and acceptor, n is the refractive index of the medium in between, R is the distance between the dipoles, and $g_d(\nu)$ and $g_a(\nu)$ are the normalized homogeneous line shapes of the donor and acceptor, respectively. The effect of the relative orientations of the dipoles is taken into account by the orientation factor κ^2 ($0\leqslant\kappa^2\leqslant4$), given by $\kappa=\mathbf{e}_d\cdot\mathbf{e}_a-3(\mathbf{e}_d\cdot\mathbf{r})(\mathbf{e}_a\cdot\mathbf{r})/|\mathbf{r}|^2$, with $\mathbf{e}$ unit vectors parallel to the donor and acceptor dipoles and $\mathbf{r}$ the vector joining the dipoles ($|\mathbf{r}|=R$).

Spectral diffusion requires that the absorption frequencies between donor and acceptor dipoles is slightly different and that the transfer process is phonon assisted. This is accounted for by the spectral overlap function in Eq. (8), which states that the excitations can be transferred as long as the (phonon-broadened) homogeneous lines overlap (see also Ref. 70). The spectral overlap between two normalized Lorentzians with equal FWHM widths $\delta\nu_{\mathrm{hom}}$ and spacing of the center frequencies of $\Delta\nu=\nu_2-\nu_1$ is

$$\int_0^\infty g_1(\nu)g_2(\nu)d\nu=\frac{1}{\pi}\frac{\delta\nu_{\mathrm{hom}}}{\delta\nu_{\mathrm{hom}}^2+\Delta\nu^2}. \tag{9}$$

As can be seen in Eq. (8), the transfer rate for an excitation depends strongly on the distance and relative orientation of the donor and acceptor dipoles. For the extensively studied faujasite structure of zeolite Y the coordinates of all the atoms are well known.[57] If the zeolite is hydrogen exchanged, the protons are distributed over three of the four crystallographically different oxygen sites in the zeolitic lattice. Protons on the O_1 sites constitute the HF absorption band and point into the supercages, whereas protons on the O_2 and O_3 sites point in the smaller sodalite cages and absorb at the LF frequencies due to hydrogen bonding.[38] For each of the three different O–H dipole sites the relative positions of the neighboring O_1, O_2, or O_3 dipole sites and the orientation factors can be calculated using the structural information.[57] The relative distances and orientation factors of the acceptor

sites within a sphere of radius 6 Å around a donor site are presented in Table II for the three kinds of oscillators. It is seen that the nearest neighbor for an O–H dipole can already be found at a distance of 3 Å.

In fully exchanged zeolite Y, which we have used in our study, not all oxygen sites are occupied by protons. For the Si/Al ratio of 2.8, in one faujasite unit cell 51 protons are distributed over 288 oxygen atoms ($O_1+O_2+O_3$). If we assume a random distribution of the protons over the possible oxygen sites, there are many possible configurations of acceptor dipoles around an excited donor dipole. The survival probability for an excitation on a donor atom which is surrounded by a number of acceptors, averaged over all possible configurations of acceptors, is given by[71]

$$\psi(t)=\left\langle \prod_i \exp[-t\xi_i k_{d\to a}(R_i,\kappa_i^2)] \right\rangle_{\{\xi_i\}}$$

$$=\prod_i \{1-p+p\ \exp[-tk_{d\to a}(R_i,\kappa_i^2)]\}, \qquad (10)$$

where ξ_i are stochastic variables, so that $\xi_i=1$ for oxygen atom i occupied with a proton and $\xi_i=0$ otherwise and p is the acceptor occupation probability. From the results of Czjeck *et al.*[57] it is inferred that in fully exchanged zeolite Y 54% of the protons is found on O_1, 9.5% is found on O_2, and 28% is found on O_3. This gives the acceptor occupation probability p for the three different oxygen sites.

It is inferred from Eq. (10) that due to the different distances and orientations, the survival probability for an excitation behaves strongly nonexponential as a function of time. Hence, a single transfer rate for the excitations cannot be calculated. However, using Eqs. (8)–(10) and the structural information given in Table II we can simulate our transient signals in the presence of Förster transfer. These calculations reveal that the excitation transfer to other frequencies is expected to occur within tens to hundreds of picoseconds. The initial excitation fraction of all Lorentzian homogeneous lines is calculated using Eqs. (2) and (3). For every time step this fraction not only decays exponentially with the vibrational lifetime T_1 [Eq. (4)], but for every homogeneous line the excitation transfer to every other homogeneous line is calculated. In one time step Δt, $[1-\psi(\Delta t)]$ of the excitation of one homogeneous line is transferred to another homogeneous line, with the transfer rate between these two lines $k_{d\to a}$ given by Eqs. (8) and (9). For p the *unexcited* acceptor occupation probability is taken (so saturation of the homogeneous lines is taken into account). This is done for all three kinds of oscillators between all homogeneous lines for each time step and in this way the excitations are redistributed by Förster transfer for every time step. The probe transmission at a certain frequency is calculated with Eqs. (5) and (7).

For the calculations of the transfer rate [Eq. (8)] a refractive index of $n=1.3$ is used[72] and for the transition dipole moments values of $\mu^{HF}=0.14$ D for the HF oscillators (on O_1) and $\mu^{LF}=0.21$ D for the oscillators on O_2 and O_3 are used. These transition dipole moments are in agreement with values calculated from integrated infrared absorbances from other experiments[73,74] and from our infrared absorption measurements, although these values have a relative accuracy of 50%. The ratio $\mu^{LF}/\mu^{HF}=1.5$ agrees with the increase of the transition dipole moment which is expected if the H bonding leads to a shift of the O–H frequency of 100 cm^{-1}.[75] In Table II it is seen that for an excitation on a HF oscillator (on O_1) there are many more possible LF acceptor sites available at close distance than at other HF sites. However, due to the spectral overlap factor in the expression for the transfer rate [see Eqs. (8) and (9)] the HF excitations will mainly migrate through the HF absorption band and only hop occasionally to the high-frequency shoulder of the LF band. It should be noted that in the calculation of the Förster transfer process there are no free adjustable parameters.

We have simulated the probe transmission as a function of delay time in the presence of Förster energy transfer for the pump and probe frequencies equal to those in the experiments shown in Fig. 13. With the signal-to-noise ratio of our time-resolved pump–probe data, the probe transmission change can only be measured over two decades at most. It is difficult to extract deviations from single exponential decay from these experimental signals and therefore only single exponential decay times τ are determined from the data (see Sec. III). To be able to compare the simulations with the measured data, the simulations are treated in an identical way: to the simulated probe transmission, which is slightly nonexponential due to the spectral diffusion process, a single exponential decay time is fitted. The results of the simulations are compared to the experiments in Fig. 13 (solid line). In the simulations a vibrational lifetime of $T_1=500$ ps is assumed for the HF oscillators to yield absorption lifetimes which correspond to the experimental data. It should be noted that in the presence of Förster energy transfer both the induced bleaching and the hot-band absorption decay faster than the T_1 lifetime, but that at the red side of the hot band the decrease in the transient absorption lifetime is smaller if the pump is at the blue side of the absorption band than if the probed oscillators are pumped resonantly. The dependence of the hot-band lifetime on center pump frequency is described well by the simulations, which strongly supports the explanation of spectral diffusion by Förster energy transfer.

One fundamental underlying assumption in the calculations of the spectral diffusion process is that for every homogeneous line the same average site distribution of surrounding oscillators (Table II) is assumed. Thus we did not account for any correlation between the center frequency of the homogeneous line and the physical position of the corresponding oscillator in the zeolite lattice (except for the discrimination between LF and HF protons in the lattice). It may well be that such a correlation between physical position and center frequency exists (in fact, that is the essence of inhomogeneous broadening), but it is not feasible to incorporate such a correlation simply because it is not known. This might explain the fact that the same simulations as represented by the solid line in Fig. 13 give a decay time for the bleaching in a one-color pump–probe experiment of $\tau=297$ ps, whereas a somewhat smaller value is observed experimentally (see Fig. 11).

Förster energy transfer between homogeneous lines in an inhomogeneous absorption band implies that a transient spectral hole which is burnt in that inhomogeneous line will broaden as a function of time. In Sec. IV A the shape of the spectral holes burnt into O–D absorption lines was found to remain constant in time (Fig. 9), proving the absence of spectral diffusion for the O–D oscillators. This is caused by the fact that for the O–D experiments the O–D oscillator concentration is only about 50% of the total hydroxyl concentration, which results in a larger average distance between the oscillators. Furthermore the transition dipole moment of the O–D is smaller than that for the O–H vibrations. Using Eq. (8) we estimate that for the O–D experiments the average transfer rate between oscillators is a factor of 8 smaller than the transfer rates in the O–H experiments. In addition, spectral diffusion has to take place before the excitations have decayed and the population lifetimes for the O–D oscillators are smaller than for the O–H vibrations. Unfortunately, the spectral width of our laser pulses at the O–H wavelength prevents an accurate determination of the transient spectral hole widths at several delay times. For excitation of the LF band a (broad) spectral hole is burnt, but the distribution of T_1 lifetimes over the band[38] complicates an interpretation of the transient spectra in terms of spectral diffusion. At the HF absorption peak the width of the bleaching is determined by the laser linewidths and the spectral resolution is too low to monitor the spectral diffusion directly.[76] However, if we take a closer look at the transient absorption data of Fig. 10, 32 ps after exact temporal overlap between pump and probe pulses, there is some bleaching visible at the high-frequency shoulder of the LF band. This shoulder cannot be explained from direct spectral overlap of the excited homogeneous bands and the probe pulse, even if a homogeneous linewidth of 5.4 cm^{-1} is taken into account. The data suggest that at this short delay time some excitations have already been transferred from the HF band to the LF band. Our simulations of the probe transmission in the presence of Förster transfer indeed show the development of LF bleaching after excitation, but at these short times the calculations underestimate this effect somewhat in comparison with the experimental data.

Using the simulations in which the spectral diffusion is modeled, the T_1 vibrational lifetimes can be estimated: at the LF absorption peak the vibrational lifetime is in the range of $50<T_1<100$ ps and for the HF O–H vibration we estimate $400<T_1<500$ ps. These lifetimes are somewhat larger than the lifetimes for the corresponding O–D vibrations, but are of the same order of magnitude. This result agrees with the ratio of O–H and O–D vibrational lifetimes of hydroxyls on SiO_2 surfaces.[16] In a forthcoming paper we will investigate the effect of isotopic exchange on the absolute values of the population relaxation rates in combination with temperature dependent studies.[77]

D. Concentration dependence

The nonradiative dipole–dipole coupling described in Sec. IV C is inversely proportional to the sixth power of the distance between the oscillators. Thus the spectral diffusion which is explained by the Förster transfer should depend strongly on the concentration of oscillators. Indicators for such a resonant coupling mechanism were indeed found in previous one-color experiments, where the transient bleaching lifetimes were found to depend on proton concentration.[38] To study the effect of oscillator concentration, parts of the O–H oscillators are exchanged for deuteration and the one-color bleaching signals are recorded for different densities. To account for heating effects (T_1 lifetimes depend intrinsically on temperature) these experiments are compared with experiments on nondeuterated samples, where the laser power was decreased to yield the same absorbed pump energy. In Fig. 14 two one-color bleaching experiments on the HF O–H vibration of zeolite Y are shown for similar absorbed pump energies. The filled dots are measured for a sample which contains all O–H oscillators and the open dots result from a sample in which 70% of the O–H hydroxyls are replaced by O–D groups, to reduce the effective oscillator concentration. It is readily observed that for the lower oscillator concentration the single-color bleaching lifetime is larger. This trend is reproduced well by our simulations which allow for spectral diffusion through dipole–dipole coupling. In both calculations represented by the lines in Fig. 14 an excited state lifetime of $T_1=400$ ps is assumed. The only difference between the two calculations is that for the dashed curve an oscillator density of 30% of the fully exchanged oscillator density (solid line) is used. It is seen that the increase in transient transmission lifetime is well accounted for by just a decrease of the concentration.

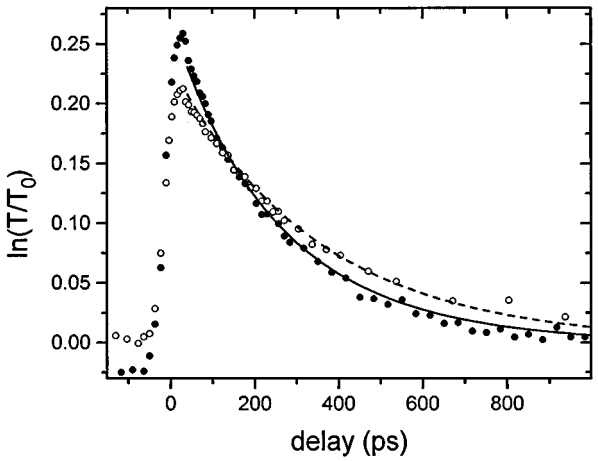

FIG. 14. Transient probe transmission as a function of the delay with respect to a pump pulse at the same frequency for the HF O–H absorption band for two different O–H oscillator concentrations. [The data have been shifted vertically so that the transmission relaxes to zero; the small finite values for the probe transmission for negative delays are due to small shifts of the absorption band after relaxation (Ref. 42)]. The bleaching clearly lives longer when the oscillator density is decreased from 100% (●, $\tau=241\pm5$ ps) to 30% (○, $\tau=358\pm11$ ps). (Similar excitation densities are chosen to prevent differences due to laser heating). The calculated curves result from the simulations of the one-color pump–probe experiment assuming a vibrational lifetime of $T_1=400$ ps and spectral diffusion through dipole–dipole coupling (see Sec. IV C). For the dashed curve the oscillator density [p in Eq. (10)] is 30% of that of the solid curve.

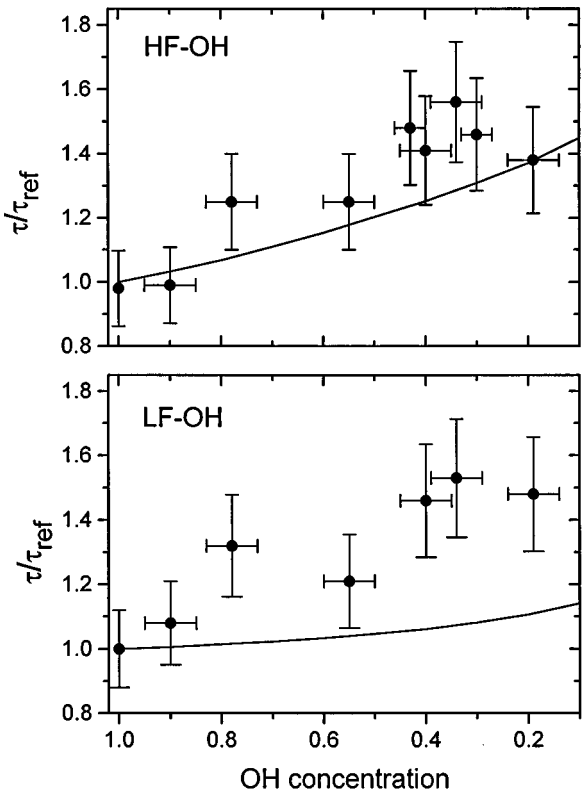

FIG. 15. One-color bleaching lifetimes for the HF (upper panel) and the LF (lower panel) absorption bands as a function of O–H oscillator concentration. The concentration is varied by partly exchanging the O–H hydroxyls with O–D oscillators, for which the vibrational frequencies are much smaller. The single exponential lifetimes for the transmission decay τ as obtained from the experiments are normalized to the decay times for fully protonated zeolite Y samples (O–H concentration=1), with the same absorbed energy per pulse, to account for differences in sample heating at different oscillator concentrations. For both absorption bands the experimental bleaching lifetimes (●) increase with decreasing oscillator densities, which confirms that at high O–H oscillator concentrations spectral diffusion of vibrational excitations mediated by a resonant transfer process takes place in these zeolites. The solid lines are the result of simulations in which (nearly) resonant transfer of the vibrational excitations (see Sec. IV C) is taken into account. The same parameters which yield the solid line in Fig. 13 are used.

The net effect (after correction for laser heating) of decreasing the oscillator concentration on the bleaching lifetimes is shown in Fig. 15. Both the bleaching lifetime for the HF absorption band and for the LF absorption band are seen to increase with decreasing proton concentration. Indeed, at high concentrations the excitations can diffuse out of the probe bandwidth, which is observed as an enhanced decay rate. If the distance between the oscillators is so large that excitation transfer cannot take place on the time scale of vibrational relaxation, population decay is the only mechanism by which the probe transmission returns to the equilibrium value. For the LF excitations the Förster transfer is faster than for the HF excitations, due to a larger transition dipole moment for the LF oscillators. The relative effect on the bleaching lifetimes, is about the same as for the HF bleaching lifetimes, because the LF vibrations have smaller T_1 population lifetimes (see Table I). The simulations, in which the same parameters are used as for the calculations of the solid line in Fig. 13 and only the oscillator concentration is varied, are found to underestimate somewhat the effect of dipole–dipole coupling on the one-color bleaching lifetimes for the LF vibration. The increase in transient transmission HF lifetime is well reproduced by the simulations.

E. Polarization diffusion

For site-to-site excitation transfer in a three-dimensional lattice like a zeolite, diffusion of the polarization of the excitations is expected. This is analogous to orientational relaxation of excited molecules in a liquid,[78–81] where the excitation polarization diffuses by the orientational motion of the excited oscillators. By probing the excited population in the polarization channels both parallel and perpendicular to the pump polarization, information about orientational motion of the excitations can be obtained.[78–81] Although the dipole–dipole transfer process has a tendency to maintain the polarization via the orientation factor κ in Eq. (8), diffusion of the polarization is expected due to the different oscillator orientations (see Table II). Especially among resonant oscillators, for which the excitation transfer rate is large due to a large spectral overlap [Eq. (9)], significant polarization scrambling is expected to occur on short time scales. In this section we investigate whether resonant Förster transfer can be identified from single-color polarization resolved pump–probe experiments.

In the setup depicted in Fig. 1 the idler beams are generated with the polarization in the plane of the paper. The polarization of the pump pulse is not affected in the pump–probe setup (Fig. 2), but due to the reflections by CaF_2 plates and the retroreflector the probe beam contains both polarization components as it impinges on the sample. In the one-color time-resolved *polarization* experiments[79] one idler beam, denoted are i1 in Fig. 2, is used for both the pump and the probe pulses (the idler beam i2 is blocked). The pump beam passes a polarizing grid filter just before it is focused onto the sample, to ensure a good linear polarization in the plane of the setup. The probe polarization is changed with a MgF_2 Babinet–Soleil compensator, which is inserted between the CaF_2 plate which splits off the reference signal and the first focusing lens in Fig. 2. With this device the probe polarization is linearized and can be changed easily from parallel to perpendicular to the pump polarization. It is checked experimentally that both pump and probe polarizations are defined better than 2%.

The results of the polarization resolved measurements, for the pump and probe frequencies resonant with the top of the HF O–H absorption band (3637 cm^{-1}), are shown in Fig. 16 for two different pump pulse energies. The probe transmission data are plotted as a function of the delay with the pump pulse for the probe polarization parallel and for the probe polarization perpendicular to the pump polarization. The pump pulse energies are 140 ± 30 μJ for the upper panel and 50 ± 10 μJ for the lower panel. It is seen that the bleaching signal in the perpendicular polarization channel for both pump energies is smaller than the bleaching in the parallel

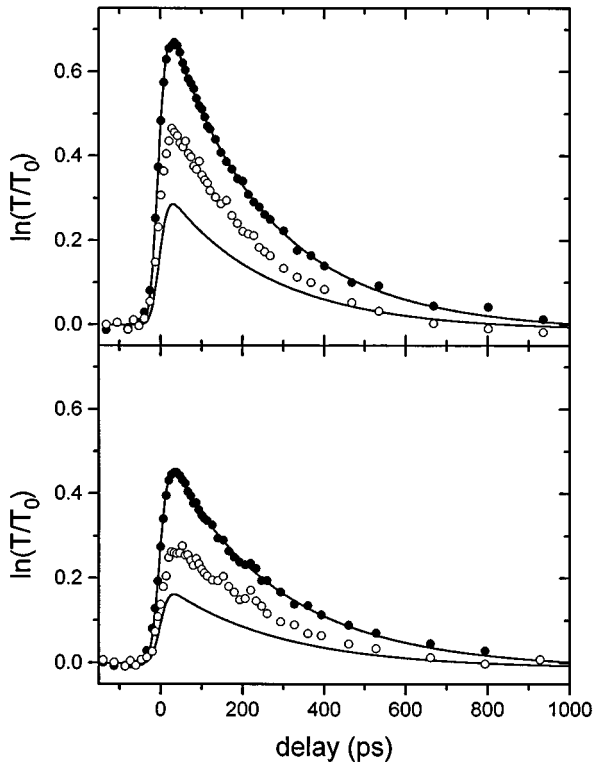

FIG. 16. One-color bleaching for a probe pulse with polarization parallel (●) or perpendicular (○) to the pump polarization as a function of time delay with the pump pulse, for two different pump pulse energies E_p. For the upper panel $E_p=140\pm30$ μJ and for the lower panel $E_p=50\pm10$ μJ. In each panel the two solid lines arise from the same calculation of the probe transmission in both polarization channels (see Appendix B), such that the calculated parallel signal corresponds to the experimental data. For the solid lines in the upper panel an exponential decay time of 272 ps is used. The pump intensity of the calculations in the upper panel has been divided by a factor of 2.1 and a lifetime of 293 ps is assumed to arrive at the solid lines in the lower panel. The crossed polarized experimental signals can be described with the same T_1 lifetimes as the parallel signals.

channel. This indicates that the polarization of the excitation is not fully isotropic, because then equal signal strengths would be observed in both channels, but is still partly oriented around the pump polarization. For both pump energies the decay times for the transmission in both polarization channels are found to be identical. This suggests that during the vibrational relaxation (after the pump pulse) no effective diffusion of *polarization* takes place. Thus polarization diffusion is either faster than our temporal resolution or much slower than the excited population lifetime. This can be resolved by comparing the bleaching amplitudes in both channels.

The anisotropy after excitation, which is defined as the ratio of the maxima of the probe transmission for both polarization channels,[79] $a=[\ln(T/T_0)]_{\parallel}^{\max}/[\ln(T/T_0)]_{\perp}^{\max}$, depends on the degree of saturation and thus on the intensity of the pump pulse. In the absence of polarization diffusion for vanishing saturation, a equals 3 (see Appendix B), but a decreases with increasing saturation.[79] We have numerically calculated the time-dependent probe transmission in both polarization channels using the differential equations which describe the excitation of transition dipoles in the sample as a function of time, distance, and orientation, see Appendix B. In these calculations polarization rotation is not taken into account, which means that all excitations keep the same orientation. The pump intensity I_0 and the population lifetime T_1 in the calculations are adapted to yield the best correspondence between the calculated and the experimental probe transmission in the parallel channel (the upper solid lines in Fig. 16). The corresponding probe transmission in the perpendicular channel from the same calculation is also shown in Fig. 16 (lower solid lines). It is clear that the experimental signals in the perpendicular channels are significantly larger than expected for a distribution of oscillators without polarization diffusion. The pump intensity in the calculations is reduced by a factor of 2.1 in going from the upper panel of Fig. 16 to the lower panel, which compares well with the ratio of the experimental pulse energies which is 2.8 ± 0.8. This confirms that we have treated the saturation effects properly and that indeed the small experimental anisotropies are *not* due to large saturations, i.e., a decrease of a due to the fact that the oscillators parallel to the pump polarization are completely bleached. The small anisotropies of the experimental signals ($a=1.4$ for $E_p=140\pm30$ μJ and $a=1.6$ for $E_p=50\pm10$ μJ) compared to the anisotropies in the calculations ($a=2.32$ and $a=2.75$, respectively) thus indicate that part of the excitations randomize faster than our 25 ps pulses during the pumping process.

The anisotropies for both experiments in Fig. 16 are a factor of 1.7 smaller than expected without polarization diffusion. A simple calculation shows that this value is obtained if about half of the excitations randomize, while the other half keeps the original $\cos\theta$ distribution. From this we conclude that during the excitation process the polarization is scrambled *partly* within our temporal resolution ($\sim$20 ps), and that the polarization anisotropy reached after excitation is maintained at later times. We explain this as follows. Part of the excited oscillators have resonant neighbors nearby and transfer of the excitation among these oscillators is fast. Because the number of nearby resonant sites for an excitation is limited, this only partly randomizes the excitation polarization. Furthermore, there are oscillators which have no resonant neighbors at small distances, so that the excitation remains there until it decays or is transferred to a nonresonant neighbor. It should be noted that the very fast *resonant* energy transfer probed in the one-color polarization experiments is consistent with the somewhat smaller rate for slightly *nonresonant* transfer found in the two-color experiments (Sec. IV B).

V. CONCLUSIONS

We have investigated the stretch vibrations of hydroxyl groups (both O–H and O–D) in acid zeolites with two-color infrared saturation spectroscopy. With this double resonance technique a wealth of information about the dynamics of these vibrations is observed. For both the LF and the HF (O–D) absorption bands transient spectral holes are burnt with the saturating pump pulse, which directly shows the

inhomogeneous character of the absorption bands. For the relatively low concentrations of O–D oscillators, for which no diffusion of the spectral excitations is observed, the homogeneous linewidth is determined from the width of these spectral holes. This yields a value for the HF and LF homogeneous linewidths of about 4 cm^{-1} for the O–D. From this a value of $\delta\nu_{hom} \simeq 5.4\ cm^{-1}$ was inferred for the O–H vibrations.

By varying the delay between the pump and probe pulses the population dynamics of the excited state is monitored directly on a picosecond time scale. For the O–D vibration the population relaxation time is found to be larger for the HF vibration ($T_1 \simeq 123$ ps) than for the LF vibration ($T_1 \simeq 42$ ps), which can be explained from the hydrogen bonding of the LF oscillators (see also Ref. 38). From the values of the homogeneous linewidths and the population lifetimes, the pure dephasing times could be deduced. The homogeneous absorption linewidths are found to be completely determined by this pure dephasing time, which is about 2 ps for both hydroxylic vibrations in zeolite Y (at room temperature).

For the O–H vibrations, the high oscillator concentration and the large transition dipole moments as compared to the O–D vibrations give rise to strong dipole–dipole coupling of the vibrational oscillators in the porous lattice. Using different excitation and probing frequencies within the HF absorption band, spectral diffusion of the O–H excitations is found to take place within the inhomogeneously broadened absorption spectrum. The excitations migrate through different O–H sites, which have different absorption frequencies, and this affects the observed lifetimes of the transient signals. Due to this dipole–dipole induced transfer process, the one-color bleaching lifetime is observed to increase with decreasing O–H concentration, because the increasing average distance between the oscillators slows down the dipole–dipole transfer.

The effect of spectral diffusion on experimental transient signals is calculated using simulations in which transfer of excitations is induced by dipole–dipole coupling. In these calculations the coordinates of all oscillator sites in the zeolite lattice are used (providing the distances and orientations between the dipoles) as well as the homogeneous linewidths which were obtained from our hole-burning experiments, to account for slightly nonresonant (phonon-assisted) site-to-site transfer of the excitations. Both the pump-frequency dependence of the two-color transients and the concentration dependence of the one-color bleaching lifetime for the O–H vibrations are satisfactorily described by these calculations. From the simulations the true excited-state T_1 lifetimes for the LF O–H vibrations are estimated to be $50 < T_1 < 100$ ps, and for the HF O–H vibration we estimate $400 < T_1 < 500$ ps.

We have also performed single-color polarization resolved saturation experiments to study the role of *resonant* excitation transfer on the polarization of the excitations. After the excitation, the probe transmission in both polarization channels (parallel and perpendicular to the pump) is found to decay with the same lifetime. From the comparison of the signal amplitudes in both channels just after excitation, it is inferred that during the pump pulse the excitations are partly depolarized due to fast site-to-site transfer. The degree of isotropy reached during the excitation process is not complete because not all excitations migrate among oscillators with all orientations, because of the absence of nearby resonant O–H neighbors. The remaining anisotropy persists during the relaxation process.

ACKNOWLEDGMENTS

We would like to thank Mischa Bonn for his tremendous help throughout this study, from providing samples to useful discussions. Aart Kleyn and Rutger van Santen are also kindly acknowledged for fruitful discussions. The work described in this paper is part of the research program of the Stichting Fundamenteel Onderzoek van de Materie (Foundation for Fundamental Research on Matter) and was made possible by financial support from the Nederlandse Organisatie voor Wetenschappelijk Onderzoek (Netherlands Organization for the Advancement of Research).

APPENDIX A: EFFECTS OF SPECTRAL AVERAGING

In the conventional interpretation of the time-dependent pump–probe signals for a two-level system, it is assumed that the probe transmission change at a delay time t after an instantaneous saturating pump pulse is given by[10]

$$\ln\left[\frac{T(t)}{T_0}\right] = 2\, f_e A_0 \exp\left(-\frac{t}{T_1}\right). \tag{A1}$$

Here A_0 is the equilibrium absorbance, $A_0 = n_0 \sigma l$, with n_0 the density of (unexcited) oscillators, σ the absorption cross section per oscillator, l the optical path length, and f_e is the fraction of oscillators excited at $t=0$ by the pump pulse. (In this equation and in Appendix B we assume for simplicity that the pulse duration is infinitely short compared to the relaxation time T_1, so that the time dependence of pump and probe pulses can be neglected. This treatment can be straightforwardly extended with the explicit time dependencies of the laser pulses). However, Eq. (A1) is only valid for one excited fraction f at one frequency and can only be applied without restrictions to situations where the laser linewidth is much smaller than the *homogeneous* absorption band.

In general, in time-resolved infrared saturation spectroscopy, the linewidths of pump and probe pulses are comparable to the absorption bandwidths. Then it is necessary to treat the frequency dependences explicitly. In most experiments, the transmitted probe pulses are not detected in a spectrally resolved manner, but the measured probe transmission is a spectral average over the probe bandwidth and the transmitted probe energy in absence of the pump pulse reads

$$T_0 = \int T_{pro}(\nu) \exp[-A_0(\nu)]\, d\nu, \tag{A2}$$

where $T_{pro}(\nu)$ is the input probe energy. For a purely homo-

geneous absorption band the excited fraction over the band is constant and does not depend on frequency. For an inhomogeneously broadened absorption band however, the distribution of excited fractions over the absorption band is determined by the spectral content of the pump pulse [see Eq. (2)], so in general we must write $f(t)=f(t,\nu)$ and the probe transmission after the pump pulse is given by

$$T(t)=\int T_{\mathrm{pro}}(\nu)\exp\{-A_0(\nu)[1-2\,f(t,\nu)]\}d\nu. \tag{A3}$$

Using the time dependence of the excited fraction as given in Eq. (4), the experimentally determined transmission change for the probe is given by

$$\ln\left[\frac{T(t)}{T_0}\right]=\ln\left[\frac{\int T_{\mathrm{pro}}(\nu)\exp\{-A_0(\nu)[1-2\,f_e(\nu)\exp(-t/T_1)]\}d\nu}{\int T_{\mathrm{pro}}(\nu)\exp[-A_0(\nu)]d\nu}\right], \tag{A4}$$

and now the relation $\ln[T(t)/T_0]\sim\exp(-t/T_1)$ is not obvious due to the integration over frequency. (Note that we have assumed that T_1 is independent of frequency within the probe bandwidth, which is not necessarily the case for an inhomogeneous absorption band). This proportionality is recovered in the limit $2\,f_e(\nu)A_0(\nu)\ll 1$ because then the probe transmission may be approximated by

$$T(t)\simeq\int T_{\mathrm{pro}}(\nu)\exp[-A_0(\nu)]\times\left[1+2A_0(\nu)f_e(\nu)\exp\left(-\frac{t}{T_1}\right)\right]d\nu. \tag{A5}$$

This gives

$$\ln\left[\frac{T(t)}{T_0}\right]\simeq\ln\left[1+\exp\left(-\frac{t}{T_1}\right)\times\frac{\int T_{\mathrm{pro}}(\nu)2\,\exp[-A_0(\nu)]f_e(\nu)A_0(\nu)d\nu}{\int T_{\mathrm{pro}}(\nu)\exp[-A_0(\nu)]d\nu}\right], \tag{A6}$$

which, due to the assumption $2\,f_e(\nu)A_0(\nu)\ll 1$ which was made above in Eq. (A5), can be approximated by

$$\ln\left[\frac{T(t)}{T_0}\right]\simeq\exp\left(-\frac{t}{T_1}\right)\times\frac{\int T_{\mathrm{pro}}(\nu)\exp[-A_0(\nu)]2\,f_e(\nu)A_0(\nu)d\nu}{\int T_{\mathrm{pro}}(\nu)\exp[-A_0(\nu)]d\nu}. \tag{A7}$$

This has the desirable delay-time dependence and predicts a single exponential decay as a function of t for the transmission change.

The difficulty with the constraint $2\,f_e(\nu)A_0(\nu)\ll 1$ is that it implies that the bleaching signal is small [see, e.g., Eq. (A1)], whereas for saturation spectroscopy the bleaching should be significant in order to detect the decay as a function of delay time. For larger saturation levels, the Taylor expansion made in Eq. (A5) cannot be truncated after the first term, but reads

$$T(t)\simeq\int\left\{T_{\mathrm{pro}}(\nu)\exp[-A_0(\nu)]\times\left[1+2A_0(\nu)f_e(\nu)\exp\left(-\frac{t}{T_1}\right)+\frac{4}{2!}A_0^2(\nu)f_e^2(\nu)\exp\left(-\frac{2t}{T_1}\right)+\cdots\right]\right\}d\nu, \tag{A8}$$

and terms in the probe transmission appear which decay with T_1, $\frac{1}{2}T_1$, $\frac{1}{3}T_1$, etc. This should not be a problem because from the experiments $\ln[T(t)/T_0]$ is determined and the logarithm should recover the single $\exp(-t/T_1)$ dependence (because obviously $\ln[\exp(x)]=x$ for all values of x). However, the integration over the different frequencies spoils this scheme. Due to the finite spectral widths of the pump pulse and the absorption band, for some frequencies which are within the probe linewidth the restriction $2\,f_eA_0\ll 1$ holds, but for other frequencies this approximation is not valid and an expansion like Eq. (A8) has to be used. In a one-color experiment in which the pump and probe pulses are tuned to the maximum of the absorption band, the largest values of $2\,f_eA_0$ will be found at the center frequencies of the laser pulse. These large values necessitate taking the higher order terms in Eq. (A8) into account, but the large and small signals are integrated with weighting factors $T_{\mathrm{pro}}(\nu)\exp[-A_0(\nu)]$. The spectrally integrated signal may then be small enough to make the approximation for the logarithm as done in Eq. (A7) still valid. Thus due to the integration of large and small signals at different frequencies, the logarithm in Eq. (A6) does not fully balance the faster decaying terms. As a result, the measured transmission change for the probe, $\ln[T(t)/T_0]$, is found to decay *faster* than single exponentially with T_1.

For the induced hot band the situation is analogous, but leads to *slower* observed decays. The population fraction which is excited to the $v=1$ excited level can be promoted to the $v=2$ level, and consequently an induced absorption hot band is found at the $v_{1\rightarrow 2}$ transition frequency. At the fundamental transition, the population *difference* is twice the excited population, but at the hot-band transition the population difference equals the excited population (see Fig. 3). The frequency integrated transmission for a probe at the induced hot-band reads [compare Eq. (6)] as follows:

$$T(t)=\int T_{\mathrm{pro}}(\nu)\times\exp\left\{-\beta A_0(\nu+\nu_{\mathrm{anh}})f_e(\nu+\nu_{\mathrm{anh}})\exp\left(-\frac{t}{T_1}\right)\right\}d\nu, \tag{A9}$$

where the parameter β accounts for the effect that the transition dipole moments of the $v_{1\rightarrow 2}$ and the $v_{0\rightarrow 1}$ transition are different in general ($\beta=2$ for a harmonic oscillator). The full expression for the experimentally determined transmission change of a probe at the hot-band frequency is given by [see Eq. (A4)]

$$\ln\left[\frac{T(t)}{T_0}\right]=\frac{\int T_{\mathrm{pro}}(\nu)\exp\{-\beta A_0(\nu+\nu_{\mathrm{anh}})f_e(\nu+\nu_{\mathrm{anh}})\exp(-t/T_1)\}d\nu}{\int T_{\mathrm{pro}}(\nu)d\nu}, \tag{A10}$$

where we have assumed that in equilibrium there is no absorption at the hot-band frequency. The Taylor expansion of Eq. (A9) for the probe transmission at the hot-band frequency is given by

$$T(t)\simeq\int\left\{T_{\mathrm{pro}}(\nu)\left[1-\beta A_0(\nu+\nu_{\mathrm{anh}})f_e(\nu+\nu_{\mathrm{anh}})\exp\left(-\frac{t}{T_1}\right)+\frac{\beta^2}{2!}A_0^2(\nu+\nu_{\mathrm{anh}})f_e^2(\nu+\nu_{\mathrm{anh}})\exp\left(-\frac{2t}{T_1}\right)-\cdots\right]\right\}d\nu. \tag{A11}$$

Two important differences with respect to Eq. (A8) should be noted. First, the sign of the first term in the transmission change (with T_1) is opposite the first term in Eq. (A8), which just expresses that at the fundamental frequency the transmission is increased, whereas at the hot-band frequency the transmission is decreased. However, the higher-order terms in Eq. (A11) have alternating signs opposed to Eq. (A8). Thus with increasing saturation, the next term which becomes important, with time-constant $\frac{1}{2}T_1$, is a fast decaying transmission *increase* at the hot-band frequency. Analogous to the one-color experiment, if the probe is tuned to the center of the hot band, this effect will contribute relatively strongly to the transient signal. As a consequence, from combining a transmission decrease with T_1 and a smaller transmission increase which decays with $\frac{1}{2}\ T_1$, $\ln[T(t)/T_0]$ decays *slower* than single exponential decay with T_1.

The second important difference between Eqs. (A8) and (A11) is that in the expression for the fundamental absorption an additional factor $\exp[-A_0(\nu)]$ is found, which is absent for the induced hot band. This is of importance for the spectral shapes of the induced transmission changes. For every excitation fraction, no matter how small, the probe transmission at the fundamental frequency is given by [see Eq. (A3)]

$$T_{0\rightarrow 1}(t)=\int T_{\mathrm{pro}}(\nu)\exp[-A_0(\nu)]\exp[2A_0(\nu)f(t,\nu)]d\nu. \tag{A12}$$

At the hot-band frequency we have

$$T_{1\rightarrow 2}(t)=\int T_{\mathrm{pro}}(\nu)\exp[-\beta A_0(\nu+\nu_{\mathrm{anh}})f(t,\nu+\nu_{\mathrm{anh}})]d\nu. \tag{A13}$$

(The reference transmission values T_0, which are the transmissions without the pump pulse, are given by the same equations with $f(t,\nu)=0$). If the sample is optically thin, the factor $\exp[-A_0(\nu)]$ in Eq. (A12) may be approximated by 1. Then the same shape and amplitude are found for the spectral hole as for the hot band, when the probe frequency is scanned over both spectral features. For an optically thick sample however, the frequency dependence of $\exp[-A_0(\nu)]$ must explicitly be taken into account before the integration over all frequencies within the probe bandwidth is performed. When the pump pulse is tuned to the center of the absorption band, the value of $\exp[-A_0(\nu)]$ has a minimum at the frequencies which have the largest bleaching. This suppresses the effect of the large bleaching at the top of the absorption band compared to the wings, and the transmission increase for a probe at the center of the absorption band is smaller than the transmission decrease at the center of the induced hot band. This is again due to the fact that the integration over the probe bandwidth takes place in the experiment before the logarithm acts on the transmitted probe signal. Thus for optically thick samples (which is usually the case for saturation spectroscopy), the amplitude of the bleaching is suppressed compared to that of the hot band, because at the frequency where the transmission change is large the probe is absorbed most. The spectral width of the bleaching is also affected by this effect. The exact manifestation depends on the specific frequency dependencies of A_0, f, and T_{pro}.

Let us summarize what we have shown in this Appendix. In time-resolved saturation spectroscopy the probe pulses which are transmitted by the sample are usually detected in a spectrally integrated way. If the linewidth of the probe pulse becomes comparable to any other spectral width in the system (homogeneous linewidth, inhomogeneous absorption width), the transient signals may differ from the intuitively expected signals and care has to be taken in the interpretation. If within the probe linewidth for some frequencies the relation $2\,f_eA_0\ll 1$ holds, whereas this is not valid at other probed frequencies, transient contributions to the probe transmission with shorter lifetimes start to become important. In general this means that at the fundamental absorption

the probed decay of the bleaching is faster than single-exponential decay with T_1, whereas at the hot-band frequency a decay slower than a single-exponential decay with T_1 is found. Equal lifetimes for the bleaching and hot-band absorption lifetimes, like we found for the O–D experiments (Sec. IV A), suggest that these effects are not important for the O–D vibrations. To be sure however, the spectral integration of the probe transmission should be accounted for using the equations given above. We have done this and for the O–D experiments it was indeed found that the transmission-change lifetimes could be identified with T_1 population lifetimes. At the O–H vibration the larger laser linewidth necessitates this analysis to extract energy decay times. It should be noted that the homogeneous linewidth within the inhomogeneous absorption band should be known to perform this analysis, because the frequency dependence of f is given by the spectral overlap between homogeneous lines and the pump pulse [see Eqs. (2) and (3)]. In addition to this effect on the lifetimes of the transient signals, for optically thick samples the amplitude and shape of the induced bleaching may differ from the amplitude and shape of the induced hot band. This effect is even present at vanishing excitation levels. To get around this problem, the spectral contents of pump and probe pulses should again be treated explicitly, as was done both in this Appendix and in Sec. III.

APPENDIX B: CALCULATION OF THE POLARIZED SIGNALS

To calculate the probe transmission for the probe polarization both parallel and perpendicular to the pump polarization in the absence of polarization diffusion (see also Ref. 79), we assume a two-level system for which the upper level has a population lifetime T_1. (Spectral diffusion is neglected in these calculations.) For a saturating pump pulse with intensity $I(t_p)=I_0 i(t_p)$, where $i(t_p)$ is the normalized time dependence, which travels in the x direction through a sample and is polarized in the z direction, the population that can absorb the light is given by the following differential equations (in the coordinate frame of the moving light pulse):

$$\frac{\partial \Delta n(x,t_p,\theta,\phi)}{\partial t_p} = -k_{01} i(x,t_p)\Delta n(x,t_p,\theta,\phi)\cos^2\theta + k_{10}[1-\Delta n(x,t_p,\theta,\phi)], \tag{B1}$$

$$\frac{\partial i(x,t_p)}{\partial x} = -\alpha \Delta n(x,t_p,\theta,\phi) i(x,t_p)\cos^2\theta, \tag{B2}$$

where θ is the angle between the oscillator transition dipole and the pump polarization, ϕ is the corresponding azimuthal angle, $\Delta n(x,t_p,\theta,\phi)=\Delta N(x,t_p,\theta,\phi)/N_{\mathrm{tot}}$ is the fraction of unexcited oscillators oriented along (θ,ϕ) which can absorb the light (N_{tot} is the total number of oscillators) and α is the absorption coefficient, $\alpha=A_0/l=\sigma\rho$ where l is the length of the sample, σ is the absorption cross section per oscillator, and ρ is the density of oscillators. The upward rate is given by $k_{01}=2\sigma I_0/h\nu$ and the relaxation rate is the inverse of the excited state lifetime, $k_{10}=1/T_1$. The initial angular distribution of the transition dipoles is assumed to be isotropic, which is valid for the zeolite powder samples because there is a random orientation of crystalline grains in these samples. Equations (B1) and (B2) are solved numerically and this gives the fraction of oscillators which can absorb the probe pulse, $\Delta n(x,t_p,\theta,\phi)$. This distribution of available oscillators can be integrated over the sample thickness and both angles to yield the fraction of oscillators available to absorb the probe in the two polarization channels (parallel and perpendicular to the pump):

$$\begin{aligned}\Delta N_{\parallel}(t_p) &= \frac{1}{4\pi l}\int_{x=0}^{x=L}\int_{\phi=0}^{\phi=2\pi}\int_{\theta=0}^{\theta=\pi}\Delta n(x,t_p,\theta,\phi)\times\cos^2\theta\sin\theta\,d\theta\,d\phi\,dx\\ &= \frac{1}{2l}\int_{x=0}^{x=L}\int_{\theta=0}^{\theta=\pi}\Delta n(x,t_p,\theta)\times\cos^2\theta\sin\theta\,d\theta\,dx,\end{aligned} \tag{B3}$$

$$\begin{aligned}\Delta N_{\perp}(t_p) &= \frac{1}{4\pi l}\int_{x=0}^{x=L}\int_{\phi=0}^{\phi=2\pi}\int_{\theta=0}^{\theta=\pi}\Delta n(x,t_p,\theta,\phi)\times[1-\cos^2\theta]\sin\theta\sin^2\phi\,d\theta\,d\phi\,dx\\ &= \frac{1}{4l}\int_{x=0}^{x=L}\int_{\theta=0}^{\theta=\pi}\Delta n(x,t_p,\theta)\times[1-\cos^2\theta]\sin\theta\,d\theta\,dx.\end{aligned} \tag{B4}$$

For both cases ΔN reduces to $\frac{1}{3}$ for $\Delta n(x,t_p,\theta)=1$, which corresponds to an unexcited isotropic distribution of oscillators. Note that for vanishing pump intensity the oscillators are excited according to a $\cos^2\theta$ distribution around the pump polarization, for which we obtain $[\frac{1}{3}-\Delta N_{\parallel}(t_p)]/[\frac{1}{3}-\Delta N_{\perp}(t_p)]=\frac{1}{3}$, which is expected for an initially isotropic distribution of oscillators excited with a linearly polarized pump field in the absence of rotational relaxation (see also Ref. 79).

The treatment presented so far is valid for one frequency component. To account for all the effects described in Appendix A it should be extended to a distribution of homogeneous absorption bands, but this would complicate the calculations significantly. For the HF O–H absorption band, for which the laser linewidth is broader than the absorption band and the homogeneous linewidth is *not* very much smaller than the inhomogeneous linewidth (see Table I), it is reasonable to assume that the excited fraction f_e does not depend on frequency. Hence, the absorption band is treated as homogeneous and Eqs. (B1)–(B4) are solved using one *effective* absorption coefficient α (or cross section σ) and one pump intensity I_0. The probe transmission as a function of the delay t with respect to the pump, for a homogeneous

band with a frequency independent excited fraction given by Eqs. (B3) and (B4), is now calculated as a spectral average [compare Eq. (A3)]:

$$T_x(t)=\int T_{\mathrm{pro}}(\nu)\exp[-3A_0(\nu)\Delta N_x(t)]d\nu, \tag{B5}$$

where $x=\|$ for the probe polarization parallel to the pump polarization and $x=\perp$ for the perpendicular channel [the factor of 3 is inserted to cancel the $\frac{1}{3}$ which is obtained for ΔN in Eqs. (B3) and (B4) for $\Delta n(x,t_p,\theta)=1$]. In this way the transient probe transmission $\ln[T(t)/T_0]$ is calculated for both polarization channels and can be compared to the experimental signals. Note that the spectral averaging effect described in Appendix A is accounted for in these calculations. In the calculations for the HF O–H oscillators we have used an oscillator density of $\rho=5\times10^{26}$ m^{-3} and a sample length of $l=50$ μm. The absorption coefficient was determined from the experimental absorption spectrum. It should be noted however that the oscillator density can be changed by one order of magnitude without significantly changing the calculated transmission transients if the pump intensity I_0 is adapted to yield the same magnitude of the bleaching.

[1] A. Laubereau and W. Kaiser, Rev. Mod. Phys. **50**, 607 (1978).
[2] J. Chesnoy and D. Ricard, Chem. Phys. Lett. **73**, 433 (1980).
[3] J. Chesnoy and D. Ricard, Chem. Phys. **67**, 347 (1982).
[4] E. J. Heilweil, M. P. Casassa, R. R. Cavanagh, and J. C. Stephenson, J. Chem. Phys. **85**, 5004 (1986).
[5] H. Graener, R. Dohlus, and A. Laubereau, Chem. Phys. Lett. **140**, 306 (1987).
[6] H. Graener, T. Q. Ye, and A. Laubereau, J. Chem. Phys. **90**, 3413 (1989).
[7] H. Graener, T. Q. Ye, and A. Laubereau, J. Chem. Phys. **91**, 1043 (1989).
[8] H. J. Bakker, P. C. M. Planken, and A. Lagendijk, Nature **347**, 745 (1990).
[9] H. Graener, G. Seifert, and A. Laubereau, Phys. Rev. Lett. **66**, 2092 (1991).
[10] H. J. Bakker, P. C. M. Planken, L. Kuipers, and A. Lagendijk, J. Chem. Phys. **94**, 1730 (1991).
[11] H. J. Bakker, P. C. M. Planken, and A. Lagendijk, J. Chem. Phys. **94**, 6007 (1991).
[12] H. J. Bakker, J. Chem. Phys. **98**, 8496 (1993).
[13] T. Lian, B. Locke, Y. Kholodenko, and R. B. Hochstrasser, J. Phys. Chem. **98**, 11648 (1994).
[14] G. Seifert and H. Graener, J. Phys. Chem. **98**, 11827 (1994).
[15] E. J. Heilweil, M. P. Casassa, R. R. Cavanagh, and J. C. Stephenson, J. Chem. Phys. **82**, 5216 (1985).
[16] M. P. Casassa, E. J. Heilweil, J. C. Stephenson, and R. R. Cavanagh, J. Chem. Phys. **84**, 2361 (1986).
[17] R. R. Cavanagh, M. P. Casassa, E. J. Heilweil, and J. C. Stephenson, J. Vac. Sci. Technol. A **5**, 469 (1987).
[18] E. J. Heilweil, J. C. Stephenson, and R. R. Cavanagh, J. Phys. Chem. **88**, 6099 (1988).
[19] E. J. Heilweil, M. P. Casassa, R. R. Cavanagh, and J. C. Stephenson, Annu. Rev. Phys. Chem. **40**, 143 (1989).
[20] P. Guyot-Sionnest, P. Dumas, Y. J. Chabal, and G. S. Higashi, Phys. Rev. Lett. **64**, 2156 (1990).
[21] P. Guyot-Sionnest, Phys. Rev. Lett. **66**, 1489 (1991).
[22] A. L. Harris, L. Rothberg, L. Dhar, N. J. Levinos, and L. H. Dubois, J. Chem. Phys. **94**, 2438 (1991).
[23] J. D. Beckerle, R. R. Cavanagh, M. P. Casassa, E. J. Heilweil, and J. C. Stephenson, J. Chem. Phys. **95**, 5403 (1991).
[24] M. Morin, P. Jakob, N. J. Levinos, Y. J. Chabal, and A. L. Harris, J. Chem. Phys. **96**, 6203 (1992).
[25] K. Kuhnke, M. Morin, N. J. Levinos, Y. J. Chabal, and A. L. Harris, J. Chem. Phys. **99**, 6114 (1993).
[26] A. L. Harris, K. Kuhnke, M. Morin, P. Jakob, N. J. Levinos, and Y. J. Chabal, Faraday Discuss. **96**, 217 (1993).
[27] R. R. Cavanagh, E. J. Heilweil, and J. C. Stephenson, Surf. Sci. **299/300**, 643 (1994).
[28] E. J. Heilweil, M. P. Casassa, R. R. Cavanagh, and J. C. Stephenson, Chem. Phys. Lett. **117**, 185 (1985).
[29] A. Seilmeier, J. P. Maier, F. Wondrazek, and W. Kaiser, J. Phys. Chem. **90**, 104 (1986).
[30] E. J. Heilweil, Chem. Phys. Lett. **129**, 48 (1986).
[31] H. Graener, T. Q. Ye, and A. Laubereau, Phys. Rev. B **41**, 2597 (1990).
[32] H. Graener, T. Lösch, and A. Laubereau, J. Chem. Phys. **93**, 5365 (1990).
[33] U. Happek, J. R. Engholm, and A. J. Sievers, Chem. Phys. Lett. **221**, 279 (1994).
[34] I. W. M. Smith, Nature **358**, 279 (1992).
[35] M. P. Casassa, E. J. Heilweil, J. C. Stepenson, and R. R. Cavanagh, J. Electron Spectrosc. Relat. Phenom. **38**, 257 (1986).
[36] C. Hirose, Y. Goto, N. Akamatsu, J. Kondo, and K. Domen, Surf. Sci. **283**, 244 (1993).
[37] J. Kubota, M. Furuki, Y. Goto, J. Kondo, A. Wada, K. Domen, and C. Hirose, Chem. Phys. Lett. **204**, 273 (1993).
[38] M. J. P. Brugmans, A. W. Kleyn, A. Lagendijk, W. P. J. H. Jacobs, and R. A. van Santen, Chem. Phys. Lett. **217**, 117 (1994).
[39] M. J. P. Brugmans, A. W. Kleyn, A. Lagendijk, W. P. J. H. Jacobs, and R. A. van Santen, in *Time-Resolved Vibrational Spectroscopy VI*, edited by A. Lau, F. Siebert, and W. Werncke (Springer, Berlin, 1994), p. 44.
[40] M. Furuki, J. Kubota, Y. Goto, F. Wakabayashi, J. Kondo, A. Wada, K. Domen, and C. Hirose, J. Electron Spectrosc. Relat. Phenom. **64/65**, 259 (1994).
[41] M. Bonn, M. J. P. Brugmans, A. W. Kleyn, R. A. van Santen, and A. Lagendijk, in *Studies in Surface Science and Catalysis*, edited by J. Weitkamp, H. G. Karge, H. Pfeifer, and W. Hölderich (Elsevier, Amsterdam, 1994), Vol. 84, p. 493.
[42] M. Bonn, M. J. P. Brugmans, A. W. Kleyn, and R. A. van Santen, J. Chem. Phys. **102**, 2181 (1995).
[43] M. Bonn, M. J. P. Brugmans, A. W. Kleyn, and R. A. van Santen, Chem. Phys. Lett. **233**, 309 (1995).
[44] J. M. Thomas, Sci. Am. **266**, 82 (1992).
[45] G. J. Kramer, R. A. van Santen, C. A. Emeis, and A. K. Nowak, Nature **363**, 529 (1993).
[46] *Laser Spectroscopy of Solids*, 2nd ed., edited by W. M. Yen and P. M. Selzer (Springer, Berlin, 1986).
[47] *Molecular Dynamics in Restricted Geometries*, edited by J. Klafter and J. M. Drake (Wiley, New York, 1989).
[48] J. M. Drake, J. Klafter, and P. Levitz, Science **251**, 1574 (1991), and references therein.
[49] H. van der Laan, Th. Schmidt, R. W. Visschhers, K. J. Visscher, R. van Grondelle, and S. Völker, Chem. Phys. Lett. **170**, 231 (1990).
[50] H. van der Laan, C. de Caro, Th. Schmidt, R. W. Visschhers, R. van Grondelle, C. N. Hunter, and S. Völker, Chem. Phys. Lett. **212**, 569 (1993).
[51] A. Seilmeier, K. Spanner, A. Lauberau, and W. Kaiser, Opt. Commun. **24**, 237 (1978).
[52] H. J. Bakker, P. C. M. Planken, L. Kuipers, and A. Lagendijk, Opt. Commun. **73**, 398 (1989).
[53] At the O–H wavelength the bandwidth–time product for our pulses is about 60 times larger than the value for bandwidth limited pulses.
[54] W. P. J. H. Jacobs, J. H. M. C. van Wolput, and R. A. van Santen, Zeolites **12**, 315 (1992).
[55] W. P. J. H. Jacobs, J. H. M. C. van Wolput, and R. A. van Santen, Zeolites **13**, 170 (1993).
[56] W. M. Meier and D. H. Olson, *Atlas of Zeolite Structure Types* (Butterworth, London, 1987), p. 73.
[57] M. Czjzek, H. Jobic, A. N. Fitch, and T. Vogt, J. Phys. Chem. **96**, 1535 (1992).
[58] A. E. Siegman, *Lasers* (University Science Books, Mill Valley, 1986).
[59] J. Datka, M. Boczar, and P. Rymarowycz, J. Catal. **114**, 368 (1988).
[60] V. B. Kazansky, Acc. Chem. Res. **24**, 379 (1981).
[61] K. P. Schröder, J. Sauer, M. Leslie, and C. R. A. Catlow, Zeolites **12**, 20 (1992).
[62] K. P. Schröder, J. Sauer, M. Leslie, C. R. A. Catlow, and J. M. Thomas, Chem. Phys. Lett. **188**, 320 (1992).
[63] G. J. Kramer and R. A. van Santen, J. Am. Chem. Soc. **115**, 2887 (1993).
[64] Because the pure dephasing times completely determine the homogeneous linewidths, the decreasing value of T_1 with decreasing frequency in the LF absorption band cannot explain the larger homogeneous linewidth.

[65] L. M. Kustov, V. Y. Borovkov, and V. B. Kazansky, J. Catal. **72**, 149 (1981).
[66] It is assumed that the oscillators which have the smallest $v_{0\rightarrow1}$ transition frequencies in the inhomogeneous broadened line also have the lowest $v_{1\rightarrow2}$ hot-band frequencies. This is confirmed by the simulations of the transmission changes after excitation from which the homogeneous linewidths are inferred (Figs. 7 and 9). With one value for the anharmonicity of all the homogeneous lines (ν_{anh}) the (width of the) simulated induced hot band [see Eq. (6)] agrees perfectly with the data if the homogeneous linewidth is adapted to yield the right spectral width of the bleaching [using Eq. (5)].
[67] The *relative* homogeneous linewidth for the O–H oscillators is taken to be the same as for the O–D vibrations, because for the elastic interaction which determines the dephasing (the only relevant contribution to the homogeneous linewidth) the effect of the smaller mass of the oscillator is expected to be small.
[68] If the absorption spectrum is deconvoluted in homogeneous absorption lines with FWHM width smaller than 5.4 cm^{-1} even a larger variation is needed.
[69] Th. Förster, Discussions Faraday Soc. **27**, 7 (1959); in *Modern Quantum Chemistry*, edited by O. Sininoğlu (Academic, New York, 1965), Part III, pp. 93–137.
[70] T. Holstein, S. K. Lyo, and R. Orbach, in Ref. 46.
[71] J. Klafter and A. Blumen, J. Chem. Phys. **80**, 875 (1984); J. Klafter, A. Blumen, and J. M. Drake, in Ref. 47, p. 1.
[72] J. Jänchen, Ph.D. thesis, Zentralinstitut für Physikalische Chemie, Berlin, 1982.
[73] T. R. Hughes and H. M. White, J. Chem. Phys. **71**, 2192 (1967).
[74] A. Bielański and J. Datka, Bull. Acad. Polon. Sci. Sér. Sci. Chim. **22**, 341 (1974).
[75] D. Hadži and S. Bratos, in *The Hydrogen Bond*, edited by P. Schuster, G. Zundel, and C. Sandorfy (North-Holland, Amsterdam, 1976), Vol. 2, p. 565.
[76] Actually, the direct time-resolved observation of spectral diffusion of the O–H excitations could only be made using the absorption of water in the $LiNbO_3$ crystals to narrow the laser linewidth.
[77] M. J. P. Brugmans, M. Bonn, H. J. Bakker, and A. Lagendijk, Chem. Phys. (to be published).
[78] H. E. Lessing, A. von Jena, and R. Reichert, Chem. Phys. Lett. **36**, 517 (1975).
[79] H. Graener, G. Seifert, and A. Laubereau, Chem. Phys. Lett. **172**, 435 (1990).
[80] H. Graener, G. Seifert, and A. Laubereau, Chem. Phys. **175**, 193 (1993).
[81] H. Graener and G. Seifert, J. Chem. Phys. **98**, 36 (1993).